

**A REVERSE-CYCLIC ANALYSIS OF HIGH-STRENGTH CONCRETE BEAMS
WITH VARYING STEEL/FRP GRID/HYBRID REINFORCEMENT**

A Thesis

Presented in Partial Fulfillment of the Requirements for the

Degree of Master of Science

with a

Major in Civil Engineering

in the

College of Graduate Studies

University of Idaho

by

Nicholas Saras

Major Professor: Ahmed Ibrahim, Ph.D.

Committee Members: Ahmed Abdel-Rahim, Ph.D., Richard Nielsen, Ph.D.

Department Chair: Patricia J. S. Colberg, Ph.D.

May 2018

AUTHORIZATION TO SUBMIT THESIS

This thesis of Nicholas Saras, submitted for the degree of Master of Science with a Major in Civil Engineering and titled “**A reverse-cyclic analysis of high-strength concrete beams with varying steel/FRP grid/hybrid reinforcement,**” has been reviewed in final form. Permission, as indicated by the signatures and dates below, is now granted to submit final copies to the College of Graduate Studies for approval.

Major Professor: _____ Date: _____
Ahmed Ibrahim, Ph.D.

Committee Members: _____ Date: _____
Ahmed Abdel-Rahim, Ph.D.

_____ Date: _____
Richard Nielsen, Ph.D.

Department Chair: _____ Date: _____
Patricia J. S. Colberg, Ph.D.

ABSTRACT

The main goal of this study is to investigate the behavior of high-strength concrete (HSC) beams with varying steel, fiber reinforced polymer grids, and hybrid reinforcement under reverse-cyclic loading. For this experimental program, five high strength concrete beams were prepared and cast using a concrete with a 28-day compressive strength of 8.5 kips per square inch (ksi). All beams produced were 7 feet long, 9 inches tall and 8 inches wide. The control beam was reinforced with traditional Grade 60 #5 steel bars and others were reinforced with carbon fiber and glass fiber grids. Additionally, the last two beams were reinforced with steel and FRP. All beams used 2#3 Grade 60 steel rebar for top reinforcement and as stirrups, spaced at 8 inches.

The study concluded that the behavior of the HSC beams was primarily dependent on the tensile strength and modulus of elasticity of each type of reinforcement. Experimental calculations showed a decrease in moment capacity but an improvement in strength degradation for the FRP only reinforced beams compared to the steel reinforced beams. The hybrid reinforced sections showed an increase in moment capacity and ductility compared to the FRP only reinforced beams. The mechanistic model predicted values using code ACI 318 and 60% of the given FRP tensile strength as provided in ACI 440R were in relatively good agreement with the experimental results. For the hybrid reinforced beams, moment capacities calculated using ACI 440R was shown to be over-estimated. Although ACI 440R designs for externally wrapped FRP, the sectional analysis was performed with the same process as ACI 318.

Keywords: High strength concrete, fiber reinforced polymer, carbon fiber reinforced polymer, glass fiber reinforced polymer, reverse-cyclic analysis, hydraulic actuator, hysteresis loop, hysteresis curve, CFRP grid, GFRP grid, FRP grid, Shore Western Controller System, hybrid reinforcement, delamination.

ACKNOWLEDGEMENTS

To my advisor, Dr. Ahmed Ibrahim, I am grateful for the motivation, support, and academic excellence he provided me throughout my thesis and graduate studies. Working with him was an excellent opportunity of learning experience in an engineering practice sense as well as daily life advice. The patience he had for explaining difficult concepts related to this research is greatly appreciated. Without his help and continuous support this work would not have been possible. My sincere and profound thanks are due to Dr. Abdel-Rahim and Dr. Richard Nielsen for serving as members of my thesis reviewing committee.

I would also like to thank Mohammad Madaqiq and Olaniyi Arowojulu for the help they provided throughout the testing of the specimens and the guidance they provided throughout the analysis portion of testing. Also, special thanks to Don Parks for his technical support throughout the testing. Several times Don was readily available to solve any arising problem in the laboratory. This work would not have been possible without their support as well.

I wish to express my gratitude and sincere appreciation to Pre-Mix Concrete Plant in Pullman, Washington for their generous support by donating all high strength concrete and mix design materials required for this test. Without the help from Jesse Espy, manager at the Pre-Mix Concrete Plant, and the rest of their team this testing would not have been possible.

My huge appreciation to the Civil and Environmental Engineering Department at the University of Idaho for providing the necessary materials and financial support for the machines and materials required for this research. Acknowledgement is also due to the University of Idaho for the support given to this research through its facilities and for granting me the opportunity to pursue my graduate studies with financial support. I am blessed to have the wonderful opportunity to call Moscow, Idaho my home the past 7 years of my life.

DEDICATION

This work is dedicated to my father Tony Saras, my mother Mandy White, my sister Ally Saras, and all my friends here in Moscow, Idaho and all over the country for their constant guidance, encouragement and invaluable support throughout my studies. Without their moral support, this would not have been possible.

TABLE OF CONTENTS

Authorization to Submit Thesis	ii
Abstract.....	iii
Acknowledgements.....	iv
Dedication.....	v
Table of Contents.....	vi
List of Tables	ix
List of Figures.....	x
CHAPTER 1: INTRODUCTION.....	1
1.1 PROBLEM STATEMENT.....	1
1.2 OBJECTIVE OF RESEARCH.....	2
1.3 THESIS OUTLINE	2
CHAPTER 2: LITERATURE REVIEW.....	4
2.1 INTRODUCTION.....	4
2.2 DEVELOPMENT OF HIGH STRENGTH CONCRETE.....	5
2.3 DEVELOPMENT OF FIBER REINFORCED POLYMERS.....	5
2.4 FIBER REINFORCED POLYMER MATERIALS.....	7
2.4.1 Carbon Fiber Reinforced Polymer.....	10
2.4.2 Glass Fiber Reinforced Polymer.....	10
2.5 REVERSE-CYCLIC LOADING	11
CHAPTER 3: EXPERIMENTAL PROGRAM.....	13
3.1 INTRODUCTION	13
3.2 TEST OBJECTIVES	13
3.3 DESIGN OF SPECIMENS.....	13
3.4 REINFORCEMENT DETAILS	13
3.4.1 Steel Reinforcement.....	15
3.4.2 CFRP Reinforcement.....	15

3.4.3 GFRP Reinforcement.....	16
3.4.4 Hybrid Reinforcement	17
3.5 CONSTRUCTION OF SPECIMENS	20
3.6 MATERIAL PROPERTIES	21
3.6.1 Concrete.....	21
3.6.2 Reinforcement.....	22
3.7 SETTING UP.....	23
3.8 INSTRUMENTATION.....	25
3.8.1 Introduction.....	25
3.8.2 Strain Gauges.....	26
3.8.3 Data Logger	27
3.9 TEST PROGRAM.....	28
3.9.1 Introduction.....	28
3.9.2 Reverse-Cyclic Loading	28
CHAPTER 4: EXPERIMENTAL RESULTS AND DISCUSSION.....	30
4.1 INTRODUCTION	30
4.2 PERFORMANCE UNDER REVERSE-CYCLIC LOADING.....	30
4.2.1 Control Specimen (1 CONT).....	30
4.2.2 CFRP Reinforced Specimen (2 CF)	32
4.2.3 GFRP Reinforced Specimen (3 GF).....	34
4.2.4 Hybrid Steel and CFRP Reinforced Specimen (4 CF/ST).....	36
4.2.5 Hybrid Steel and GFRP Reinforced Specimen (5 GF/ST).....	38
4.3 SUMMARY OF EXPERIMENTAL RESULTS.....	41
4.4 MECHANISTIC MODEL FOR PREDICTING FLEXURAL CAPACITY OF FRP GRID REINFORCED BEAMS.....	43
4.4.1 Introduction.....	43
4.4.2 Development of Moment Capacity Models.....	44
4.4.3 Development of Deflection Capacity Model.....	47
4.4.4 Development of Ductility Model.....	48
4.4.5 Summary of Mechanistic Models.....	49

CHAPTER 5: SUMMARY AND CONCLUSIONS.....	50
REFERENCES	52
APPENDICES	55
APPENDIX-A: SHORE WESTERN CONTROLLER SYSTEM INTRODUCTORY MODULE	55
A.1 BACKGROUND	55
A.2 SYSTEM STARTUP	55
A.3 TEST SET UP.....	60
A.4 SYSTEM SHUTDOWN.....	65
APPENDIX-B: SUPPLEMENTARY DATA SHEETS FOR MATERIALS AND TESTING.....	66

LIST OF TABLES

Table 2-1: Typical FRP Material Properties.....	9
Table 3-1: Reinforcement Location Details and Geometric Properties.....	14
Table 3-2: Concrete Mix Design Material Quantities	22
Table 3-3: Reinforcement Used Strength Details [6].	23
Table 3-4: Reverse-Cyclic Loading Protocol by Max % of Beam 3 Deflection	29
Table 4-1: Summary of Load and Displacement Experimental Results.....	42
Table 4-2: Summary of Experimental Calculations	42
Table 4-3: Summary of Strain Gauge Experimental Results.....	42
Table 4-4: Beams Crack Experimental Results	43
Table 4-5: Beam Ductility Details	43
Table 4-6: Experimental and Mechanistic Models Moment Capacities.....	47
Table 4-7: Mechanistic Model Deflections	48
Table 4-8: Ductility Calculations.....	48
Table 4-9: Mechanistic Model Values versus Experimental Data	49

LIST OF FIGURES

Figure 2-1: Schematic showing fiber and matrix interaction to form an FRP composite [23]	6
Figure 2-2: Strains, stresses, and forces of a hybrid FRP/steel reinforced concrete section [23].....	7
Figure 2-3: Typical Stress-Strain Graphs of GFRP Grid, CFRP Grid and Grade 60 Steel [23]	9
Figure 3-1: Installation of Steel Strain Gauges and Reinforcement Cage for 1 Control Beam	15
Figure 3-2: Installation of Reinforcement Cage for 2 CF Beam	16
Figure 3-3: Installation of Strain Gauges and Reinforcement Cage for 3 GF Beam.....	16
Figure 3-4: 4 CF/ST Hybrid Reinforcement Cage Close-up	17
Figure 3-5: 5 GF/ST Hybrid Reinforcement Cage Close-up.....	18
Figure 3-6: Installation of Strain Gauges and Reinforcement Cage for 4 CF/ST Beam	19
Figure 3-7: Installation of Strain Gauges and Reinforcement Cage for 5 GF/ST Beam.....	19
Figure 3-8: Pre-Mix Concrete Plant unloading HSC from their truck outside BEL	20
Figure 3-9: (Top) Front, (Bottom) Cross-Section Views of Beam Geometric and Reinforcement Details	21
Figure 3-10: FRP Grid [26].	23
Figure 3-11: Schematic Diagram of Loading Frame and Specimen	24
Figure 3-12: Set-up for One Concrete Specimen (Beam 4 GF/ST).....	25
Figure 3-13: Strain Gauge Installed on the Steel Reinforcement.....	26
Figure 3-14: LVDT Installed at the Bottom of Beam Mid-span	27
Figure 3-15: Bridge Completion Module Schematic.....	28
Figure 3-16: Reverse-Cyclic Loading Protocol by Step Count.....	29
Figure 4-1: 1 CONT Hysteresis Curve	31
Figure 4-2: Beam 1 CONT Cracked.....	31
Figure 4-3: 1 CONT Failure Envelope	32
Figure 4-4: 2 CF Hysteresis Curve	33
Figure 4-5: Beam 2 CF Cracked.....	33
Figure 4-6: 2 CF Failure Envelope	34
Figure 4-7: 3 GF Hysteresis Curve.....	35

Figure 4-8: Beam 3 GF Cracked.....	35
Figure 4-9: 3 GF Failure Envelope.....	36
Figure 4-10: 4 CF/ST Hybrid Hysteresis Curve.....	37
Figure 4-11: Beam 4 CF/ST Hybrid Cracked.....	38
Figure 4-12: 4 CF/ST Failure Envelope.....	38
Figure 4-13: 5 GF/ST Hybrid Hysteresis Curve.....	39
Figure 4-14: Beam 5 GF/ST Hybrid Cracked.....	40
Figure 4-15: 5 GF/ST Failure Envelope.....	40
Figure 4-16: Stress-Strain Relationship in FRP and Steel Reinforced Beams.....	45
Figure 4-17: Stress Block Diagram for Section Analysis.....	46
Figure A-1: Pump Coolant Water Valve Open.....	56
Figure A-2: Pump Power Switches On.....	57
Figure A-3: Shore Western Pump Display.....	57
Figure A-4: Shore Western Pump Emergency Stop Button.....	58
Figure A-5: SWCS Default Startup Homepage.....	59
Figure A-6: System Startup Routine Display.....	59
Figure A-7: Shore Western Pump Pressure Gauge.....	60
Figure A-8: SWCS Hardware Tree System.....	61
Figure A-9: Test Setup to Tare Displacement and Load Values.....	61
Figure A-10: Monotonic Displacement Control Test SWCS Home Screen.....	62
Figure A-11: Reverse-Cyclic Displacement Control SWCS Home Screen.....	63
Figure A-12: Time-History Function Channel Parameters.....	64
Figure A-13: Waveform Properties for a Time-History Function.....	64
Figure B-14 Pre-Mix Concrete Plant HSC Mix Material Quantities.....	66
Figure B-15: Delphin Expert Data Logger Information Manual Display.....	67
Figure B-16: Micro Measurements LVDT Data Sheet.....	68
Figure B-17: Micro Measurements Strain Gauge Data Sheet.....	69

CHAPTER 1: INTRODUCTION

1.1 PROBLEM STATEMENT

For concrete, the primary design aspect is the maximum resistance of a concrete sample to applied pressure, also known as the compressive strength. The American Concrete Institute (ACI) defines High-Strength Concrete (HSC) as concrete with a compressive strength greater than 6,000 psi [4]. The mix material design quantities of HSC vary more compared to normal strength concrete in order to meet workability and strength requirements. However, in modern-day construction HSC is more common in structural design due to its superior durability and mechanical properties.

Furthermore, HSC reinforced with traditional steel bars has been widely used in roads, bridges, tunnels, towers, and buildings for several decades. Currently, many of these steel reinforced components in the country's infrastructure are reaching the end of their service life and have begun deteriorating at an increasing rate. One of the primary factors causing this deterioration is the corrosion of reinforcing steel inside the concrete. When the steel becomes into contact with water it will rust and expand, resulting in delamination or spalling of concrete, decreasing tensile strength, and sometimes failure. The continuing costs of maintenance on these structures led to investigations of other reinforcement materials.

With the recent advancements in materials engineering, the application of fiber reinforced polymers (FRP's) has become more common. FRP's are a relatively new class of non-corrosive, high strength, and lightweight materials, which have shown strong promise in several structural engineering applications. One of these involves the use of FRP reinforcement in concrete instead of the traditional steel bars used as reinforcement. Therefore, to promote the use of FRP in reinforcement, research in HSC reinforced with FRP, specifically, Carbon Fiber Reinforced Polymer (CFRP) and Glass Fiber Reinforced Polymer (GFRP) is needed.

To increase the service life and reduce maintenance costs of structures, CFRP and GFRP can be used as reinforcement in various structural components: bridge decks, girders, columns, beams, and footings, for example. In addition to those polymer's non-corrosive properties

which far exceed that of steel, they are extremely light, versatile, and have high tensile strength making them an ideal substitute to steel in reinforced concrete.

1.2 OBJECTIVE OF RESEARCH

The primary objective of this study is to investigate the effects of using a CFRP grid and a GFRP grid as reinforcement in HSC beams under a reverse-cyclic loading protocol, meant to mimic seismic loading. This can be achieved by testing high-strength concrete beams with various types of reinforcement: traditional steel, CFRP grid and GFRP grid, as well as steel and CFRP/GFRP hybrid, under reverse-cyclic loading protocol. The experimental data (moment capacities, strains, deflections) obtained can then be compared from beam to beam.

A secondary objective of this study is to create an introductory module for the operation of a servo hydraulic PID controller, the Shore Western Control System (SWCS) that powers the hydraulic actuator used for the reverse-cyclic loading test. This module can be used as a reference tool when using the SWCS for various types of testing. Specifically it will enable a new user to power on the actuator, successfully test (monotonic or cyclic) specimens and then power off the actuator located in the Buchanan Engineering Laboratory (BEL) Room 125. Safety steps as well as modification processes' are included in the module explanation.

1.3 THESIS OUTLINE

The thesis is divided into two parts; the first part (Chapters 2-5) presents the evaluation and analysis for the reverse-cyclic test on the FRP reinforced HSC beams and the second part (Appendix A) presents the Shore Western Controller System Introductory Module on the safe use and powering of the hydraulic actuator used for the testing in this research.

Chapter 2: “LITERATURE REVIEW”: This chapter summarizes relevant previous and existing research conducted on FRP reinforced HSC beams and on reverse-cyclic testing of concrete beams.

Chapter 3: “EXPERIMENTAL PROGRAM”: This chapter covers the experimental plan and setup for the FRP reinforced HSC beams, along with the materials used and their properties. It also provides instrumentation (strain gauges and LVDT) plan and setup.

Chapter 4: “EXPERIMENTAL RESULTS AND DISCUSSION”: This chapter describes the reverse-cyclic test results for the various FRP reinforced HSC beams. Additionally, the flexural capacity prediction models are discussed.

Chapter 5: “CONCLUSIONS AND RECOMMENDATIONS”: This chapter presents the conclusions drawn from Chapter 4. Also, recommendations are provided in this chapter for future research.

Appendix A: “SHORE WESTERN CONTROLLER SYSTEM INTRODUCTORY MODULE”: This section provides an Introductory Module on the SWCS used to power the actuator in BEL 125. Detailed explanations on the starting up and shutting down process are given as well how to run and safely perform a monotonic or reverse-cyclic test.

CHAPTER 2: LITERATURE REVIEW

2.1 INTRODUCTION

The addition of FRP's as reinforcement in HSC is a relatively recent practice that can extend the service life of a concrete structure while enhancing strength characteristics compared to that of traditional steel reinforcement. In the last 25 years or so the application of FRP's in civil engineering projects has steadily increased, likely due to the significant decrease in material and manufacturing costs [6]. Several different types and shapes of FRP materials are currently available in the construction industry, primarily unidirectional bars/strands and orthogonal grids. For purposes of tensile reinforcement of concrete, these bars and grids are used as a substitute for heavier and lower tensile strength, steel bars.

The engineering industry has a need for a substitute to steel due to its high susceptibility to corrosion, this had led to several research studies-conducted on FRP's reinforcement characteristics in HSC [4, 12, 14, 18, 22]. However, the tensile behavior of FRP is characterized by a linear elastic stress-strain relationship up to failure causing brittle failure without warning [6]. Therefore, extended research on the structural performance of hybrid FRP/steel reinforced concrete beams is necessary. Although numerous studies, [8, 12, 17, 18], have been performed on the flexural behavior of FRP and hybrid FRP/steel reinforced concrete beams, no research has been conducted on the reverse-cyclic analysis of FRP and hybrid FRP/steel reinforced HSC beams.

Reverse-cyclic analysis is often used to investigate the dynamic response of structures against repeated loads, e.g. earthquake and wind motion. The dynamic response of steel reinforced concrete specimens has been thoroughly studied in the 21st century. With the ever increasing market of FRP materials, the seismic behavior of FRP reinforced HSC members is an area of research needing more studies conducted to further understand the dynamic response provided by the FRP reinforcement.

2.2 DEVELOPMENT OF HIGH STRENGTH CONCRETE

According to the American Concrete Institute [13], HSC is defined as follows:

“A concrete that meets special performance and uniformity requirements that cannot always be achieved routinely by using only conventional materials and normal mixing, placing, and curing practices. The requirements may involve enhancements of placement and compaction without segregation, long-term mechanical properties, early-age strength, toughness, volume stability, or service life in severe environments.” HSC is typically classified as concrete with a 28-day cylinder compressive strength greater than 6,000 psi. However, ACI recognizes that the compressive strength of HSC varies geographically based on typical regional concrete strengths [16].

There are two crucial design aspects to be considered while creating a HSC mix design. The first is the low water-cement ratio required to maintain the compressive strength required. The second relates to the creation of concrete with minimal or no voids, both are facilitated by adding water-reducing admixtures (WRA's). The low water-cement ratio is typically controlled by the strength required and can cause the concrete mix to be more viscous and difficult to pour. WRA's will make the HSC more flowable and easier to pour with less voids present in the concrete structure [1].

Most of the studies found in the literature focused on the improved strength and durability of HSC. It has shown to increase long-term durability and strength throughout the design life of structures and to decrease maintenance costs while extending the service life of concrete structures [13, 16, 17]. HSC beams with various percentages of steel tensile and shear reinforcement were shown to have a greater effect on the ductility in terms of crack resistance [1].

2.3 DEVELOPMENT OF FIBER REINFORCED POLYMERS

FRP materials are made of high strength fibers embedded in a polymer matrix. The fibers have small diameters and provide the strength and stiffness of the composite. The matrix has poor mechanical properties but primarily serves to transfer loads to the fibers through shear stresses [23]. The specific properties of FRP materials vary significantly from product to product and depends on fiber and matrix shapes/orientation. In the design of FRP-reinforced concrete

structures, the reinforcement should reflect material properties similar to that required for the given concrete member. Figure 2-1 shows a typical set up of the combined fibers and matrix into a FRP composite.

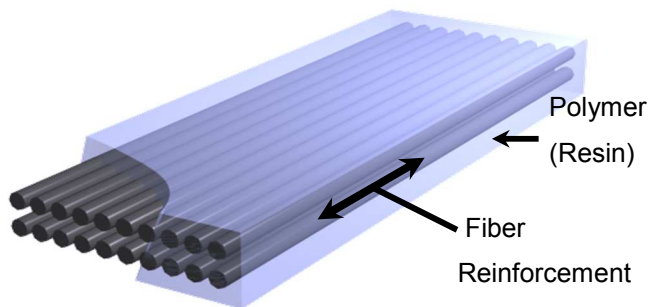


Figure 2-1: Schematic showing fiber and matrix interaction to form an FRP composite [23]

Deric Oehlers in a journal titled “FRP-Reinforced Concrete Beams: Unified Approach Based on IC Theory” [15] carried out a study on FRP and concrete internal de-bonding governed by the weak and brittle bond between the two materials. A unified approach to model the intermediate crack de-bonding was thus created and was shown to model cracks in FRP reinforced beams accurately.

Ilker F. Kara at Nigde University studied “Flexural behavior of hybrid FRP/steel reinforced concrete beams” [12] and presented a numerical method for estimating the curvature, deflection and moment capacity of hybrid FRP/steel reinforced concrete beams. Also, the numerical results indicated that beam ductility and stiffness are improved when steel reinforcement is combined with FRP reinforcement in concrete beams. This research studied normal strength concrete and thus could vary results may vary when applied to HSC. Figure 2-2 below shows the typical strains, stresses and forces of a hybrid FRP/steel bar concrete section and Equation 1 calculates the moment as a function of the tensile and compressive forces in a given section.

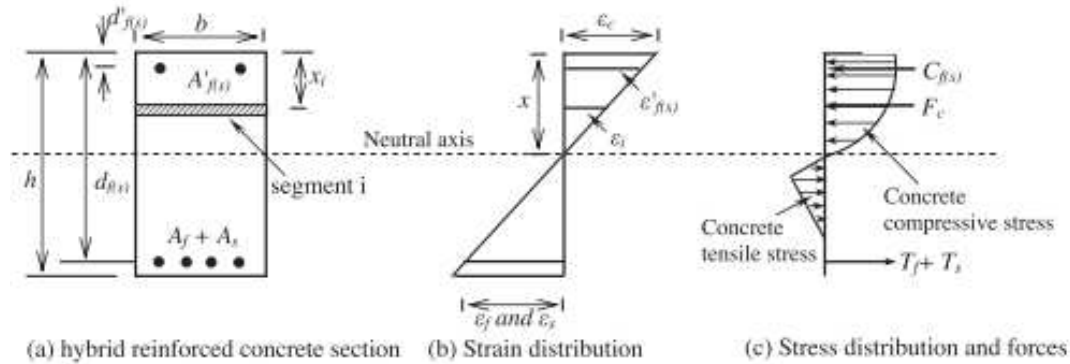


Figure 2-2: Strains, stresses, and forces of a hybrid FRP/steel reinforced concrete section [23]

$$M_f = \sum_{i=1}^n F_{ci} (x - x_i) + T_f (x - d_f) + T_s (x - d_s) + C_{f(s)} (x - d'_{f(s)}) \quad (\text{Equation 1})$$

Comparing the numerical results from Kara with experimental data proved Equation 1 to be an accurate model for the numerical calculation of a hybrid FRP/steel reinforced concrete beam [12].

Y.C. Wang conducted an “Experimental study of FRP-strengthened RC bridge girders subjected to fatigue loading” [22]. The authors presented a study on four simply supported T beams externally reinforced with GRFP and CFRP plates under monotonic and cyclic loading. It was shown that beams strengthened externally with carbon and glass laminates showed better resistance to fatigue loading than traditional steel reinforcement.

2.4 FIBER REINFORCED POLYMER MATERIALS

FRP materials have shown promising results in several engineering applications. One of these substitutes FRP reinforcing bars or grids in place of steel reinforcing bars. The primary advantage of this substitution is the non-corrosive properties of FRP materials, leading to an extended service life for concrete structures compared to steel reinforced sections [6]. An additional application of FRP materials involves the strengthening or rehabilitation of existing deteriorating or under-reinforced concrete members. FRP plates or sheets are externally bonded to concrete structures and provide necessary confinement support for the cracking or under-strength concrete.

Unidirectional FRP materials are linear elastic until failure, this differs from traditional steel which shows a defined stress yield point. Figure 2-3 on the following page shows the stress-

strain relationship between Grade 60 steel, CFRP grid and GFRP grid. Table 2-1 shows material properties of the CFRP grid and GFRP grid compared to conventional Grade 60 steel. According to [11], CFRP has the highest strength and is the most resistant to creep rupture and fatigue failure of all FRP materials. While GFRP, specifically E-Glass fiber is highly electrically resistive and is the most commonly used fiber in the reinforced polymer composite industry [11]. FRP reinforcements are commonly used in hospitals and other buildings using medical scanning equipment because they are magnetically transparent and will not interfere with the equipment.

As expected the initial construction cost for a structural component using FRP reinforcement will be higher than the costs for steel rebar reinforcement. However, these higher costs can be directly offset by two significant advantages of FRP's: the ease and speed of installation will reduce construction time and labor costs drastically and the strength-to-cost ratios can favor FRP's in certain structural elements with the extended service life generated by the FRP reinforcement. Additionally the maintenance costs using FRP's are considerably lower due to the corrosion resistant properties of the fibers [6].

Adam C. Berg performed a construction and cost analysis of an FRP reinforced concrete bridge deck, [5], and found that the construction of an FRP reinforced concrete bridge deck using conventional construction technology resulted in a 57% savings in construction labor over an identical steel reinforced bridge deck. However, as suspected the initial cost of materials for the FRP reinforced bridge was 60% higher. The long-term benefits of the more durable FRP reinforced bridge are more difficult to quantify, however maintenance costs will be reduced and the strength-to-cost ratio will not affect the overall cost of the structure.

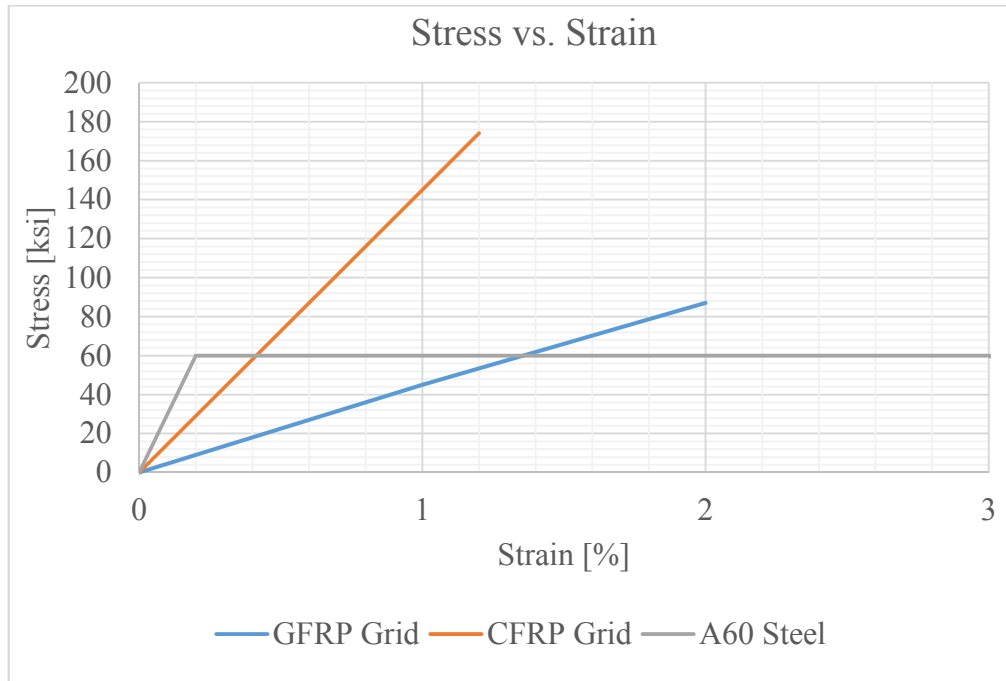


Figure 2-3: Typical Stress-Strain Graphs of GFRP Grid, CFRP Grid and Grade 60 Steel [23]

Table 2-1: Typical FRP Material Properties

Reinforcement Type	Diameter [in]	Area [in ²]	Tensile Strength [ksi]	Elastic Modulus [ksi]
Grade 60 #5 Steel Rebar	0.625	0.310	N/A	29000
V-ROD CFRP Rod	0.374	0.110	208	17400
V-ROD GFRP Rod	0.374	0.110	111	6230
NEFMAC GFRP Grid	N/A	0.122	87	4350
NEFMAC CFRP Grid	N/A	0.155	174	14500
NEFMAC AFRP Grid	N/A	0.143	189	7830

As shown in Figure 2-3 and Table 2-1, FRP materials typically have higher tensile strengths than conventional steel. However, the modulus of elasticity is most always less than steel's, and this can lead to formation of large cracks in or unserviceable deflections in certain

concrete members. As a result serviceability considerations (cracking and deflection) control the design of the FRP reinforced concrete element.

The ductility of FRP reinforced concrete beams can be increased by using a hybrid, i.e. FRP and steel combined, reinforcement [12]. One study, [12], used software analysis to locate the optimal hybrid location for a hybrid FRP and steel reinforced concrete beam. By placing the steel closer to the middle of the beam, the FRP provides adequate tensile support near the bottom of the beam and the steel adds to the ductility of the beam. Additionally, by placing the steel rebar further from the concrete, increasing the concrete cover, the steel will be less exposed to the salt and water, leading to less corrosion and cracking. The potential for a sudden brittle failure is also relieved.

2.4.1 Carbon Fiber Reinforced Polymer

Carbon fiber has the largest range of strength and stiffness of all commonly used structural FRP's. Typically carbon fibers are split into categories based on its modulus of elasticity: low, standard, intermediate, high, and ultra-high modulus [11]. The use of prefabricated CFRP bars and grids is limited to straight or slightly curved surfaces, for example, beams, columns and bridge decks [21]. Additionally, carbon fibers have a high-resistance to thermal, chemical, and environmental effects. Unlike traditional steel, FRP's will not rust and expand when in contact with salt/water [6]. Justin Jar, Bridge Inspection Manager at the Utah Department of Transportation, [14], provided an approximate unit cost for CFRP to be \$30 - \$50 per square foot including labor and material costs in 2014. Table 2-1 shows material properties of the NEFMAC CRFP grid used in this research.

2.4.2 Glass Fiber Reinforced Polymer

Glass fibers are the least expensive FRP material and, therefore, are the most commonly used fiber in structural engineering applications. GFRP's are often used in non-weight-critical structures that can tolerate larger deflections resulting from their low elastic modulus. E-Glass fiber is the most commonly used and the cheapest fiber in the industry and has a high electrical resistance [6]. Justin Jar, Bridge Inspection Manager at the Utah Department of Transportation, [14], provided an approximate unit cost for GFRP to be \$20 per square foot including labor and material costs in 2014. Similarly to carbon fiber, glass fiber is non-

corrosive and will not rust when in contact with salt and water. Additionally, GFRP is more heat resistant than CFRP and can be applied externally or internally to fire hazard structures [23]. Table 2-1 shows material properties of the NEFMAC GRFP grid used in this research.

2.5 REVERSE-CYCLIC LOADING

According to [7], a “cyclic load” is the repeated loading and unloading of a specimen. It was found that the specimen would break after a certain number of cyclic loads, even though the maximum cyclic stress applied was much lower than the ultimate strength of the material. This behavior is known as fatigue and is related to the reverse-cyclic loading. There are three types of cyclic loading defined, [7], as the following:

- 1) Zero-to-max-to-zero: A part of the member carrying no load is then subjected to load, and then the same load is unloaded back to zero.
- 2) Varying loads superimposed on a constant load: Similar to the first type however the specimen has a constant load applied rather than returning to zero. An example of this is suspension wires holding a bridge deck.
- 3) Fully-reversing load: Loading in which a tensile stress of some value is applied to unloaded part and then released, then a compressive stress of the same value is applied and released. This type has the same function form as type 1, except it oscillates to the same loading values in the opposite direction.

A few tests have been performed on the seismic performance of HSC beams. Fang, Xue, and Xiao, [9, 24, 25], conducted tests on HSC beam specimens subjected to various types of cyclic loading. Fang, [9], studied 15 cantilever HSC beam specimens and found that HSC beams under cyclic loads had slower strength degradation and better energy dissipation compared to normal strength concrete. Xue, [25], studies indicate that the normal strength beams behave in a more ductile manner compared to pre-stressed beams under reverse cyclic loading. Lastly, Xiao, [24], performed an experimental and analytic seismic performance of large scale high strength concrete beams. The HSC beams exhibited increased capacity and improved hysteretic performance compared to normal strength concrete under positive moment.

Very little research has been performed on the behavior of FRP reinforced concrete beams subject to reverse cyclic loading. M. K. Sharbatdar, [20], explored the characteristics of a large

scale cantilever FRP reinforced concrete beam tested under cyclic loading. It was found that hysteretic relationship of flexure controlled FRP reinforced beams experience stiffness degradation under cyclic loading, due to progressive cracking of the concrete, compared to traditional steel reinforced sections. No research has been published on the reverse-cyclic analysis of FRP reinforced HSC beams.

CHAPTER 3: EXPERIMENTAL PROGRAM

3.1 INTRODUCTION

In this chapter, the details of the experimental program conducted at the “Buchanan Engineering Laboratory” at the University of Idaho (UI) are discussed and reported. The test comprised of five HSC beams with dimensions of: 7 feet long, 8 inches wide and 9 inches high. The five beams have varying steel, CFRP grids, GFRP grids, and hybrid reinforcement and were tested under a displacement controlled reverse-cycle regime. The aims of the test are to study the reverse-cyclic behavior of the reinforced HSC beams and the effectiveness of the CFRP grids, GFRP grids, and hybrid reinforcement used internally as tensile reinforcement. All of the test specimens had the necessary equipment and instruments to measure and record data from the experiment.

3.2 TEST OBJECTIVES

The objectives of the experimental program are to:

1. Understand and study the behavior of beams made with high strength concrete under reverse-cyclic loading.
2. Study the effectiveness of CFRP grids, GFRP grids and hybrid CFRP/steel and GFRP/steel reinforcement used in the HSC beams.

3.3 DESIGN OF SPECIMENS

In the experimental program, the design of each member was designed to fit the fixed support and hydraulic actuator set up located in the Buchanan Engineering Laboratory (BEL). The design of each element was done to replicate traditional-to-modern building beams and bridge beams in low seismic region. There are currently no ACI codes or design guides for concrete beams internally reinforced with FRP materials.

3.4 REINFORCEMENT DETAILS

From the literature review on factors responsible for mode of failure of FRP reinforced concrete sections, it was observed that the FRP material will not yield and consequently will

allow for sudden brittle failure. Therefore, the beams were designed to have more ductility and relieve the brittle failure mode by using a hybrid FRP grid and steel combination. The beams had the same top reinforcement and shear reinforcement, also known as vertical stirrups, throughout the entire experimental program. The bottom reinforcement varied from beam to beam and will be further discussed in this chapter's section.

Table 3-1 on the following page gives the reinforcement detailing for each beam. The top reinforcement is the same for each beam and has 2 #3 Grade 60 steel rebar. The vertical stirrups are also #3 Grade 60 steel rebar spaced at 8 inches on center. The reinforcement ratio, shown in Equation 2 below, is the ratio of the area of reinforcement, A_R , to the cross-sectional area of the section, A , and is also given in Table 3-1 for each beam.

$$\rho = \frac{A_R}{b*d} \quad (\text{Equation 2})$$

For FRP reinforced concrete sections, it is recommended to over-reinforce the design because the material has no defined yield point, [11]. However, a limiting factor in this experiment was FRP material available. All reinforcement ratios fall under the ACI 318-11 code recommended reinforcement ratio. There is currently no ACI code established for a recommended value of FRP reinforcement ratios. Typically for the type of steel used in this experiment the maximum reinforcement ratio is given as 0.02 per ACI 318-11.

Table 3-1: Reinforcement Location Details and Geometric Properties

Type	Beam Name	Bottom Reinforcement Details	Area [in²]
Control Specimen	1Cont	2 #5 G60 Steel rebar	0.620
CFRP Grid	2CF	1 row - CFRP grid	0.310
GFRP Grid	3GF	1 row - GFRP grid	0.244
CFRP + Steel	4CF/ST	2 #5 G60 Steel rebar + 1 row - CFRP grid	0.930
GFRP + Steel	5GF/ST	2 #5 G60 Steel rebar + 1 row – GFRP grid	0.864

3.4.1 Steel Reinforcement

The first beam used as a control beam had a steel formwork cage with three steel strain gauges as shown in Figure 3-1. The first strain gauge was located at the mid-span of one of the #5 steel rebar used as the bottom reinforcement. Additionally, two steel strain gauges were placed on each end vertical stirrup. A fourth strain gauge was placed externally on the concrete at the mid-span.



Figure 3-1: Installation of Steel Strain Gauges and Reinforcement Cage for 1 Control Beam

3.4.2 CFRP Reinforcement

The second beam, 2CF, had one layer of CFRP grid as bottom reinforcement. Figure 3-2 below shows the reinforcement cage used. Two strain gauges were placed at the CFRP grid mid-span as well as one steel strain gauge placed at one vertical stirrup end, for a total of 3 strain gauges used in beam 2 CF. Additionally, an external concrete strain gauge was placed at mid-span.



Figure 3-2: Installation of Reinforcement Cage for 2 CF Beam

3.4.3 GFRP Reinforcement

Figure 3-3 below shows the installation of strain gauges and reinforcement cage for the third beam, 3 GF, which was reinforced with a glass fiber grid. This beam had 3 strain gauges. The first was located at the mid-span of the GFRP grid, the second at the vertical stirrup end and the last was used to measure the concrete strain and was externally placed at the mid-span of the beam.



Figure 3-3: Installation of Strain Gauges and Reinforcement Cage for 3 GF Beam

3.4.4 Hybrid Reinforcement

The last two beams utilize a hybrid of FRP and steel as reinforcement in the HSC. To ensure a hybrid connection between the FRP grid and steel bars, metal ties connected the steel bars on top of the grids, between the vertical stirrups, as shown for the CFRP and GFRP in Figures 3-4 and 3-5, respectively. By placing the steel bars further from the concrete beam edge, i.e. increasing the steel reinforcement concrete cover, the steel will also be less susceptible to corrosive damage from rusting [23]. Although this experimental program did not test this factor, it has been proven in previous research that providing FRP as tensile reinforcement and steel reinforcement located closer to the center of the beam, ductility will increase compared to only FRP reinforcement and strength and durability will be improved compared to placing the FRP material in the bottom [12].



Figure 3-4: 4 CF/ST Hybrid Reinforcement Cage Close-up



Figure 3-5: 5 GF/ST Hybrid Reinforcement Cage Close-up

Figure 3-6 shows the strain gauge and reinforcement cage installations for the fourth beam, 4 CF/ST, which has 2 #5 steel rebar above a single row of CFRP grid as bottom reinforcement. Likewise Figure 3-7 on the following page shows the strain gauge and reinforcement cage for the fifth beam, 5 GF/ST that utilizes a similar hybrid set up except using a GFRP grid instead of a CFRP grid. To ensure uniformity the steel rebar was fixed to the FRP material in the bottom reinforcement using metal ties. Beam 4 CF/ST had four strain gauges. The first strain gauge was attached to the #5 steel bar at the mid-span, the second two were attached to the CFRP at mid-span on either end of the grid. Additionally, a concrete strain gauge was placed at mid-span.

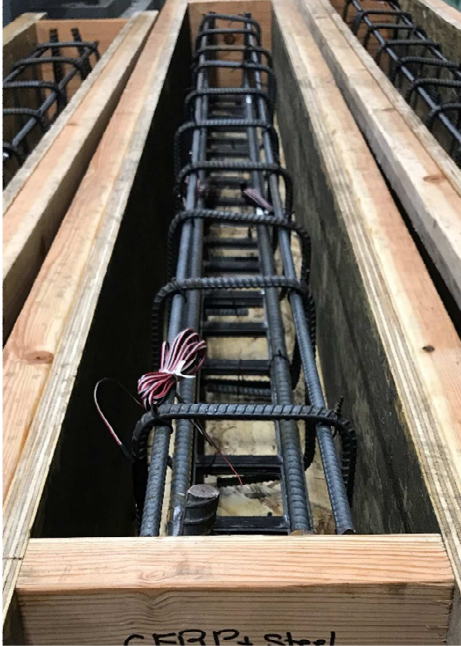


Figure 3-6: Installation of Strain Gauges and Reinforcement Cage for 4 CF/ST Beam

Figure 3-7 shows the installation of the strain gauges for beam 5 GF/ST. In total four strain gauges were used for this beam. Two located at the mid-span of the GFRP grid on either end of the row, one located at the #5 bar mid-span and the last strain gauge externally placed on the concrete at mid-span.



Figure 3-7: Installation of Strain Gauges and Reinforcement Cage for 5 GF/ST Beam

3.5 CONSTRUCTION OF SPECIMENS

The HSC beams were cast in the BEL structures laboratory using high strength concrete donated from Pre-Mix Concrete Incorporated located in Pullman, Washington. Figure 3-8 on the following page shows the Pre-Mix concrete truck in final mixing before pouring into the wheel barrow to be hauled in the BEL lab for pouring into formworks. Wooden formworks were produced according to the dimensions required for the specimens, with provision of the desired concrete cover, 1 inch, on all sides of the beam using plastic seats. Figure 3-9 gives the structural details of the beams as well as the locations of the reinforcements throughout the beam. In total eight vertical stirrups spaced at 8 inches center-to-center were used as both shear reinforcement as well as to hold the reinforcing cage (bottom and top reinforcement) together using metal ties.

During reverse-cyclic loading the tension and compression sides of the concrete's cross section are flipped when the protocol reverses the load, thus requiring reinforcement in both the top and bottom portions of the beam. Due to limited material quantities, FRP reinforcement is used only as bottom reinforcement for this experimental program.



Figure 3-8: Pre-Mix Concrete Plant unloading HSC from their truck outside BEL

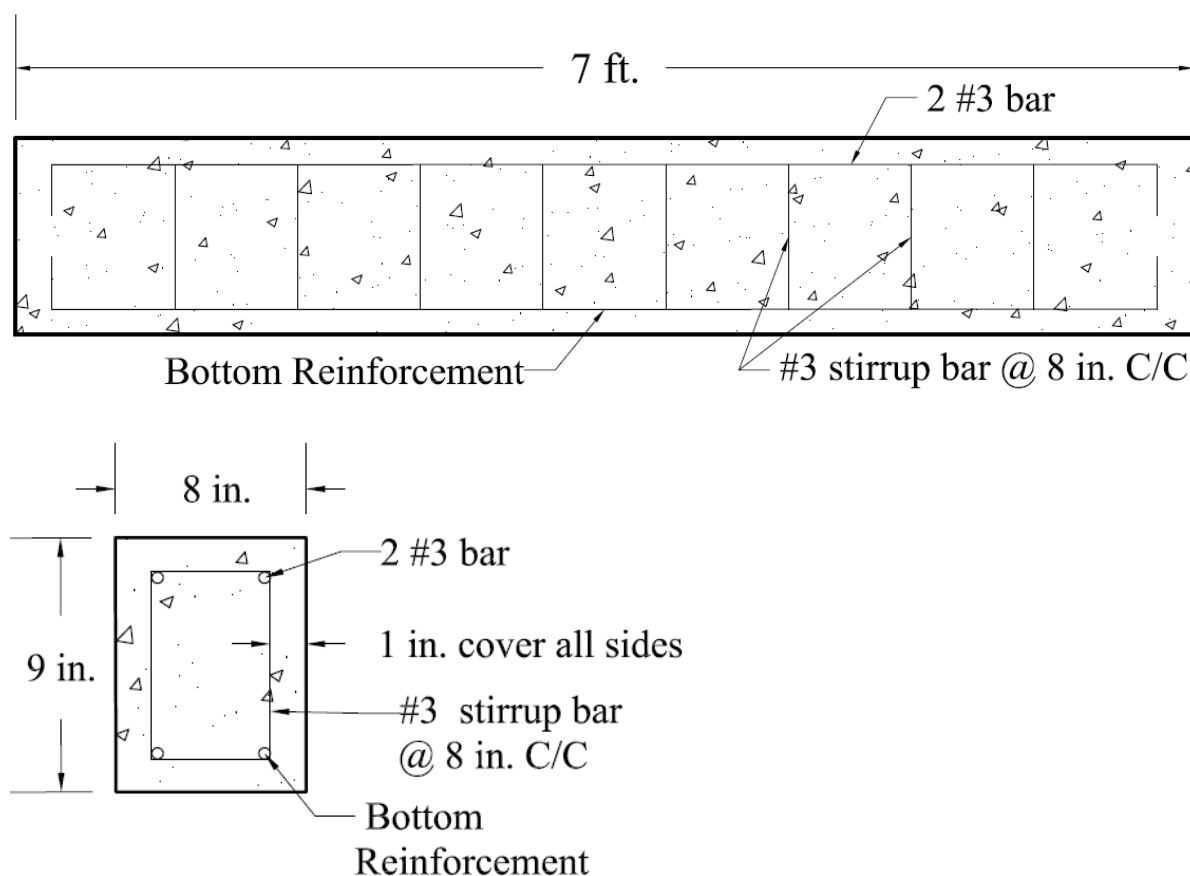


Figure 3-9: (Top) Front, (Bottom) Cross-Section Views of Beam Geometric and Reinforcement Details

3.6 MATERIAL PROPERTIES

3.6.1 Concrete

The high-strength concrete was graciously donated from the Pre-Mix Concrete plant, with a targeted strength of 10 ksi. In total 1.75 cubic yards of HSC was donated for this experiment. Two 4-inch diameter by 8-inch height cylindrical samples were taken from the batch used for the beams to conduct 28th day compressive strength test according to ASTM standards. The average 28th day compressive strength came to be 8.5 kips per square inch (ksi). The lower strength of our concrete slightly lowered our predicated moment capacities, but not significantly. Table 3-2 shows the material quantities batched by Pre-Mix for this concrete mix. A water-to-cement ratio of 0.329 resulting in a 4 inch slump was produced by this mix. Air-entrainer, Daravair, was used as well as a water reducing agent, Daracem. HSC mix designs typically demand water reducing agents to maintain the strength while keeping the water-to-cement ratio low while providing a more flowable concrete. Additionally, this will

decrease voids in the concrete as the concrete flows around the formwork easier. To limit air voids a concrete vibrator was used while pouring the beams.

Table 3-2: Concrete Mix Design Material Quantities

Material	1 yd³		1.75 yd³	
	Design		Batched	
<i>Coarse - 3/4"</i>	1725	lb	3018.75	lb
<i>Fine - Blend Sand</i>	1450	lb	2537.5	lb
<i>Cement (Type I-II)</i>	846	lb	1480.5	lb
<i>Daravair</i>	3	oz	5.25	oz
<i>Daracem</i>	50	oz	87.5	oz
<i>Water</i>	33	gal	58.4	gal

3.6.2 Reinforcement

From the literature review and as shown in Table 3-3, it is known that FRP materials do not yield. They also have a significantly lower modulus thus they experience substantially larger deflections compared to traditional steel rebar. NEFMAC FRP grids consist of carbon fibers saturated in vinyl resin with a rough fiber volume of approximately 40%. The GFRP grid, for example, has 5% carbon fiber, 39% glass fiber and 56% resin by volume [26]. The carbon and glass fibers are manufactured to form a 2D orthogonal grid with symmetrical mechanical properties as shown in Figure 3-10. Another notable characteristic from Table 3-3 is the strength-to-weight ratio of the FRP materials compared to steel. This design aspect is often used to mitigate the high initial cost of FRP reinforcements [14].

Table 3-3: Reinforcement Used Strength Details [6].

Reinforcement Type	Area [in ²]	Tensile Strength [ksi]	Elastic Modulus [ksi]	Yield Stress [ksi]	Strain at Break [%]	Weight [lbs/ft]
G60 #5 Steel Rebar	0.310	100	29000	60	0.14-0.25	1.043
NEFMAC CFRP Grid	0.155	174	14500	N/A	0.5-1.9	0.525
NEFMAC GFRP Grid	0.122	87	4350	N/A	1.2-3.1	0.292

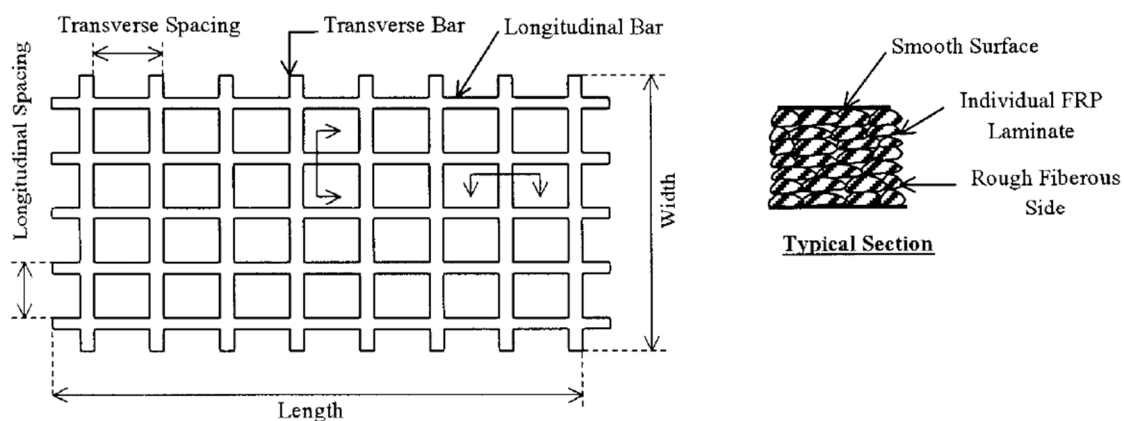


Figure 3-10: FRP Grid [26].

3.7 SETTING UP

The test setup available in the structures lab located at UI in the BEL has been designed to simulate the forces and boundary conditions that occur during seismic action in buildings and bridges.

In this model, the left and right ends of the beam are fixed to supports welded to the frame set up in the lab. The welded supports allow for a minimum of 7-foot specimens to be properly connected placed on top of them. The mid-span of the beam allows for load reversal that is typical experience in seismic loading.

The test was conducted using a steel reaction loading frame connected to BE with a hydraulic actuator hanging vertically from the top of the frame. The load cell in this hydraulic actuator

has a maximum capacity of 50,000 pounds to run the reverse-cyclic test the Shore Western Control System (SWCS). According to the Shore Western website, [Servo], this controller system “is an industry-leading customizable servo hydraulic PID controller with command optimization.” Appendix A is an Introductory Module describing the powering, operation, and test running of the SWCS located in BEL.

Figures 3-11 and 3-12 show the schematic diagram of the frame and beam 4 GF/ST in the given testing procedure. All beams were loaded with the same geometric configurations. As shown the beam is fixed at the supports as well as the actuator to the beam at mid-span.

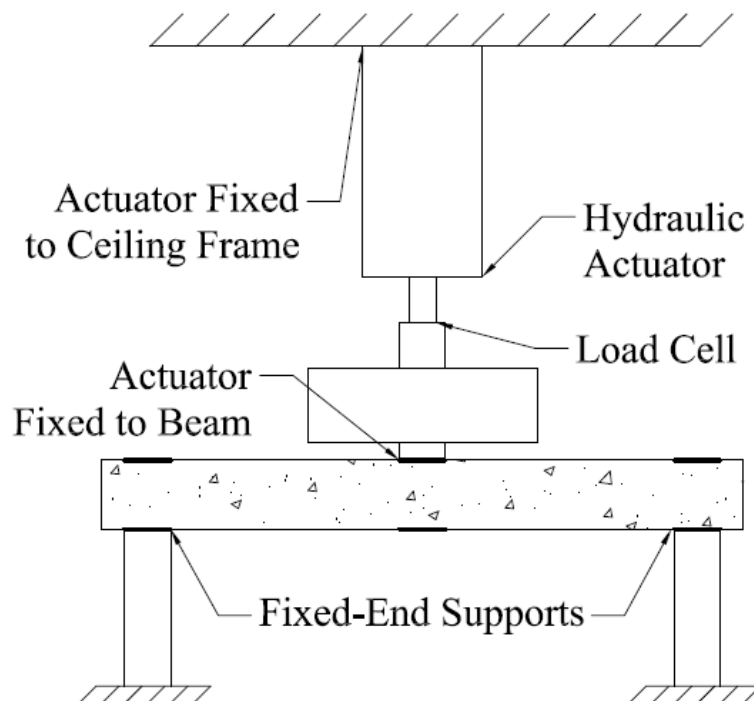


Figure 3-11: Schematic Diagram of Loading Frame and Specimen



Figure 3-12: Set-up for One Concrete Specimen (Beam 4 GF/ST)

3.8 INSTRUMENTATION

3.8.1 Introduction

All of the specimens were designed to capture the necessary testing information required for the study. This information includes strains in concrete, steel and FRP reinforcement, beam mid-span displacement, and load applied. The instrumentation was completed in two stages. The first was completed during specimen reinforcement cage construction, which involved fixing the strain gauges to the reinforcement before pouring concrete. The second was completed in the lab prior to the test by fixing the external equipment to the loaded specimens, such as the Linear Variable Differential Transformer (LVDT) which measures deflection at the bottom mid-span of the beam, as well as the concrete strain gauges placed externally on the hardened concrete at mid-span.

3.8.2 Strain Gauges

3.8.2.1 Stage One: Fixing of Reinforcement Strain Gauges

In this stage of instrumentation, Micro-Measurements™ strain gauges of 350 Ω electrical resistance capacity were attached to the mid-span of all bottom reinforcements used in the beams. The surface of the steel/FRP grids were cleaned with baking soda and vinegar and smoothed out to create a proper fixation surface for the strain gauge. They were glued to the surface using epoxy and then left 24 hours to dry. Next, self-fusing tape was used to protect the strain gauges from moisture and other potential distresses experienced from pouring of the concrete. Strain conditioners were attached to all gages to magnify the millivolt output of the gage and the gage factors were input into the data logger as specified by the manufacturer. The same capacity strain gauges were installed in at least one end vertical stirrup as well. Figure 3-13 details the strain gage fixation to the steel reinforcement.



Figure 3-13: Strain Gauge Installed on the Steel Reinforcement

3.8.2.2 Stage Two: Fixing of Concrete Strain Gauges and LVDT

In this stage, an LVDT, a 350-ohm strain gauge bridge to sense movable rod displacement, and concrete strain gauges were installed. Micro-Measurements™ also supplied the linear displacement sensor, a model HS50 with a maximum full-scale displacement of 3 inches. The LVDT was used to monitor deflection of the beam at the mid-span, the same location of loading. The LVDT location can be seen in Figure 3-12 and up close location in Figure 3-14.



Figure 3-14: LVDT Installed at the Bottom of Beam Mid-span

3.8.3 Data Logger

,Delphin Technology's Expert Logger 200, supporting 32 analog input channel up to a 1 kHz sample rate with 4/8 digital inputs/outputs, was used to collect and log the data obtained from the strain gauges and LVDT. The data logger can process up to 46 analog input channel at high sampling rates with a resolution impedance equal to 24Bit/1G Ω . After connecting the sensors to the data logger as shown in Figure 3-15, the gage factors could be input, which would convert the voltage from the sensor to the necessary output. To complete this circuit a bridge completion module had to be designed and created to connect the sensor and the logger appropriately. The detailing of the bridge completion module is shown in Figure 3-15. The Expert Logger provided a 10V excitation external source which allowed for the test to have a maximum of 5 sensors (strain gauges and LVDT's) per beam.

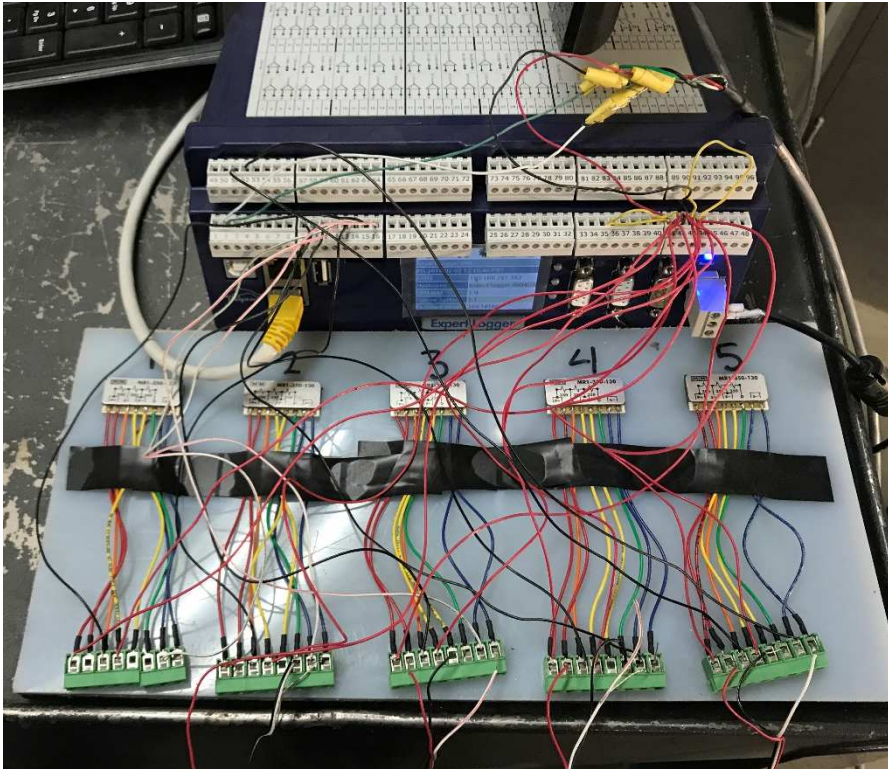


Figure 3-15: Bridge Completion Module Schematic

3.9 TEST PROGRAM

3.9.1 Introduction

In this study, reverse-cyclic tests were performed to study the behavior of hybrid FRP reinforced HSC beams. In total 5 reverse-cyclic tests were conducted in this study. The displacement controlled loading protocol used for testing will be discussed in this section.

3.9.2 Reverse-Cyclic Loading

Five specimens were tested under reverse-cyclic regime, using displacement controlled protocol. The test was used to simulate actual seismic activity that occurs in real life for buildings and bridges. The loading was applied using protocol shown in Table 3-4 and Figure 3-16. The same loading protocol was applied for all specimens.

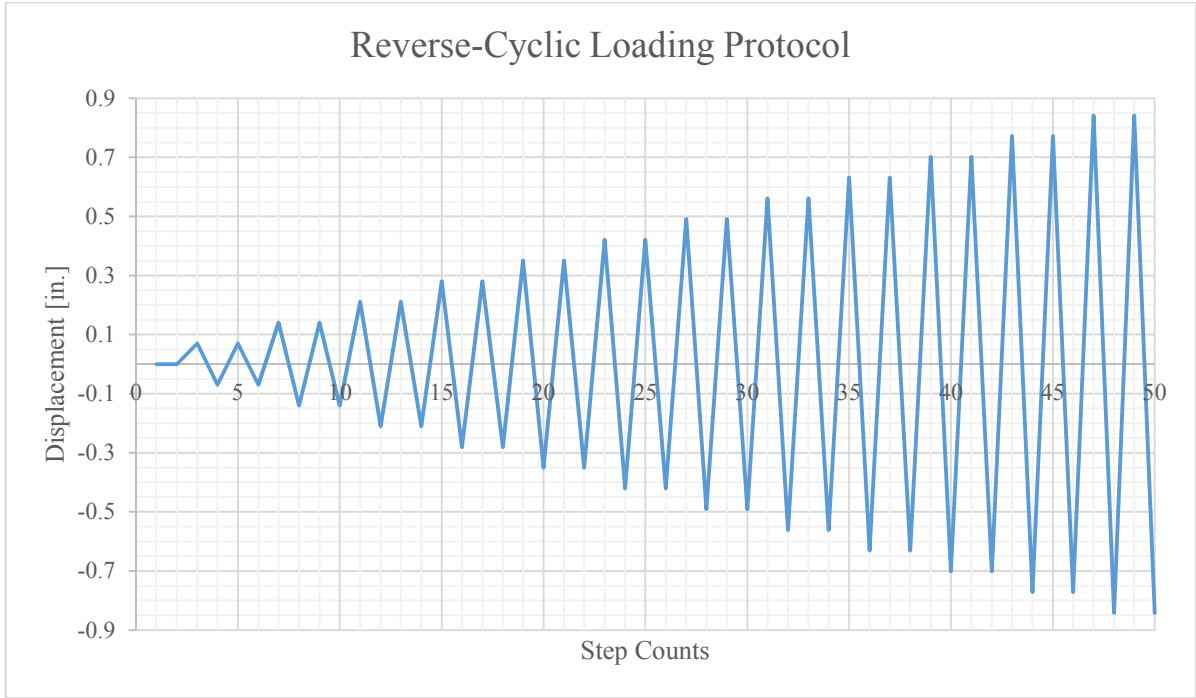


Figure 3-16: Reverse-Cyclic Loading Protocol by Step Count

Table 3-4: Reverse-Cyclic Loading Protocol by Max % of Beam 3 Deflection

Cycle	Push [in.]	Pull [in.]	[%] of Max Deflection (Beam 3)
1	0.0701	-0.0701	10%
2	0.1403	-0.1403	20%
3	0.2104	-0.2104	30%
4	0.2806	-0.2806	40%
5	0.3507	-0.3507	50%
6	0.4209	-0.4209	60%
7	0.4910	-0.4910	70%
8	0.5612	-0.5612	80%
9	0.6313	-0.6313	90%
10	0.7015	-0.7015	100%
11	0.7716	-0.7716	110%
12	0.8418	-0.8418	120%

CHAPTER 4: EXPERIMENTAL RESULTS AND DISCUSSION

4.1 INTRODUCTION

This chapter discussed the outcomes of the experimental program described in Chapter 3. The major aim of the experiment is to investigate the behavior of hybrid FRP reinforced HSC beams. The parameters to be discussed and monitored are crack spacing and width, load-displacement hysteresis curve, and ductility. These parameters were recorded and compared for each beam with varying reinforcement.

4.2 PERFORMANCE UNDER REVERSE-CYCLIC LOADING

4.2.1 Control Specimen (1 CONT)

This specimen was tested under reversed cyclic loading using a displacement controlled regime. The first crack was observed at a load of 7.9 kips in the push direction corresponding to a displacement of 0.1415 inches. This specimen had the fewest amount of cracks with an average crack spacing of about 5.72 inches and an average crack width approximately equal to 0.25 inches.

During the testing process the flexural crack at mid-span became wider. The bottom reinforcement steel yielded before the concrete failed at a strain value of 0.0334 corresponding to a load of 20.02 kips in the pull direction. The steel reinforcement reaching its yield strain led to failure of the sample by flexure. The ultimate damage mode for the specimen and the load-displacement hysteresis curve are shown in Figure 4-1 and Figure 4-2.

The failure envelope for this specimen can be seen in Figure 4-3. The ductility index for this specimen is approximately equal to 2.64 and is also shown in failure envelope, Figure 4-3. The calculation of the ductility index will be further detailed in this chapter.

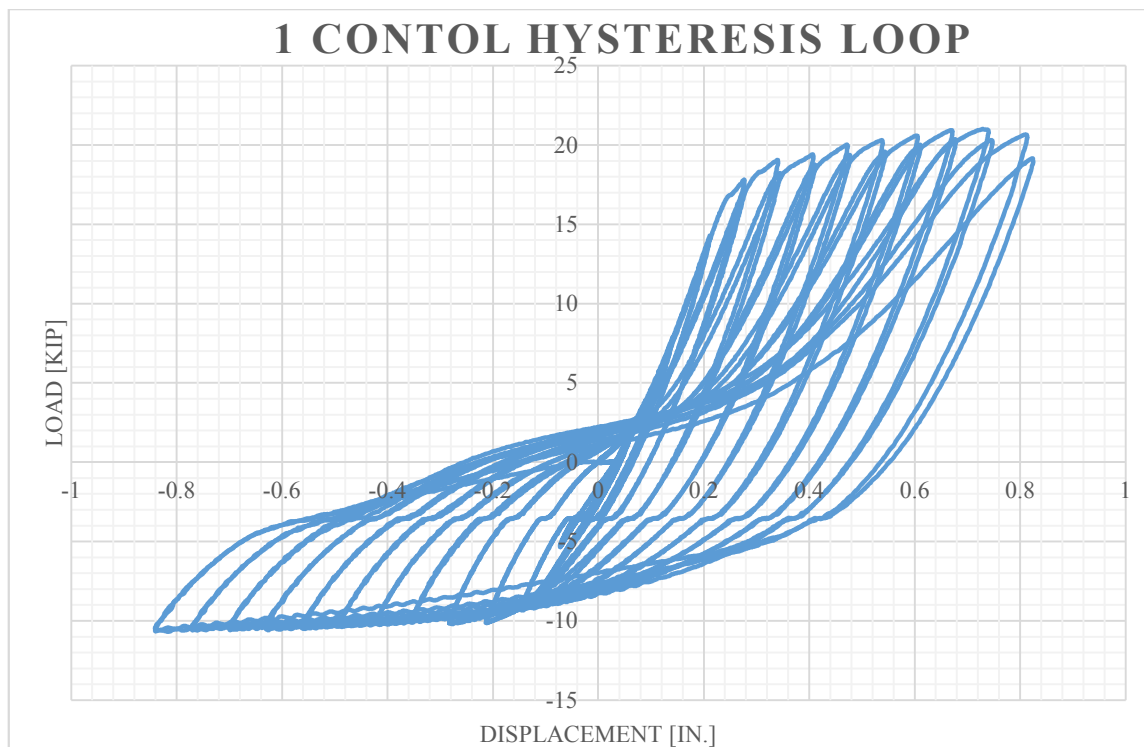


Figure 4-1: 1 CONT Hysteresis Curve



Figure 4-2: Beam 1 CONT Cracked

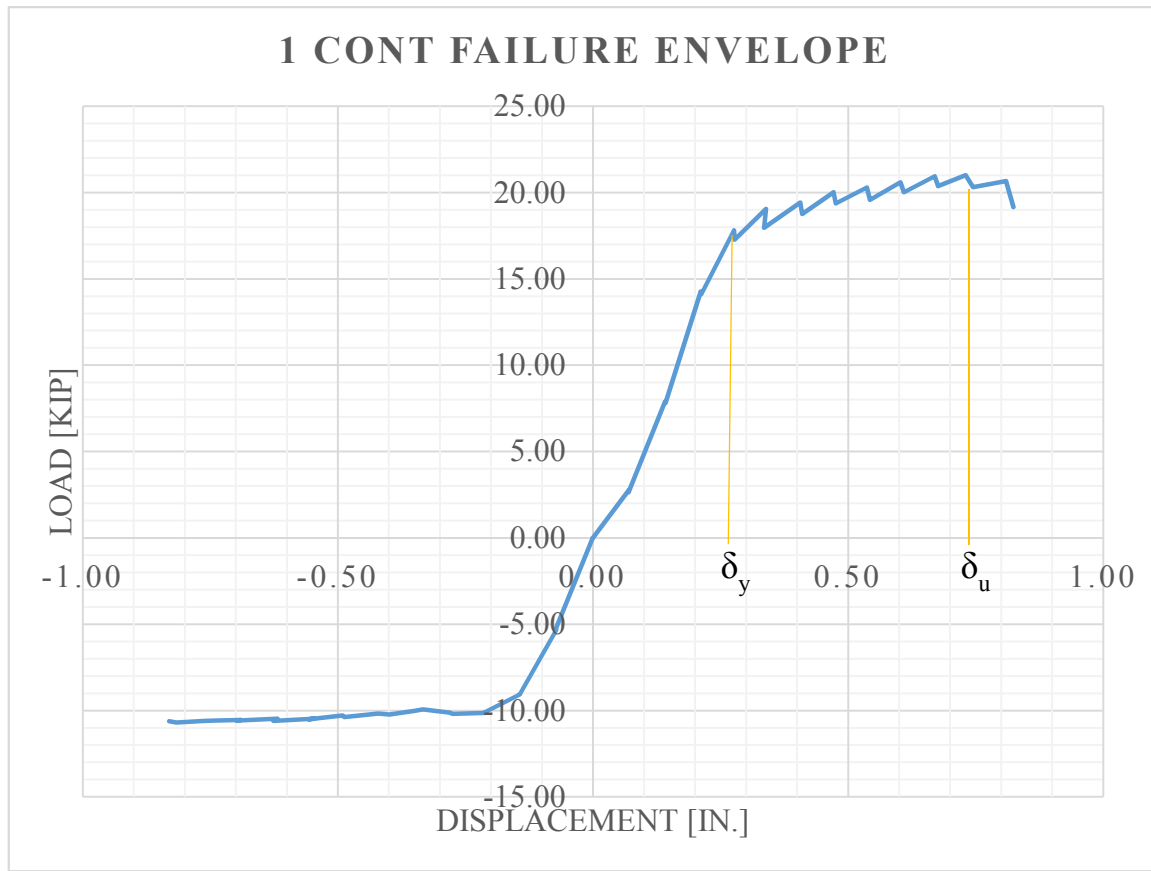


Figure 4-3: 1 CONT Failure Envelope

4.2.2 CFRP Reinforced Specimen (2 CF)

In this specimen, one row of CFRP grid was used as reinforcement in the bottom portion of the beam and tested under reverse-cyclic loading using a displacement controlled regime. The first crack was observed at load of 4 kips corresponding to a displacement of 0.2085 inches in the push direction. The cracks were spaced fairly evenly at an average of 6.2 inches with an average crack width of 0.101 inches. The CFRP delaminated at a load of 19.64 kips corresponding to a CFRP strain value of 0.0357. A small shear crack is observed near the left end support of the beam at a load of 7 kips, however the strain in the stirrup did not reach the yield strain.

As the test continued, the flexural crack at the mid-span of the beam became wider and the CFRP in this region delaminated as the strain in the CFRP exceeded its ultimate strain. This rupture led to the failure of the sample by flexure as shown in Figure 4-4 and Figure 4-5.

The failure envelope for this specimen can be seen in Figure 4-6. There is no ductility index ($\mu = 0$) for this specimen because the CFRP grid reinforcement does not yield, as shown in the failure envelope, Figure 4-6. As expected the ductility index for this specimen is zero due to the more brittle CFRP grid material used as reinforcement. For this experimental program the ultimate strain ($\epsilon_{u,c}$) of the CFRP was used in calculations.

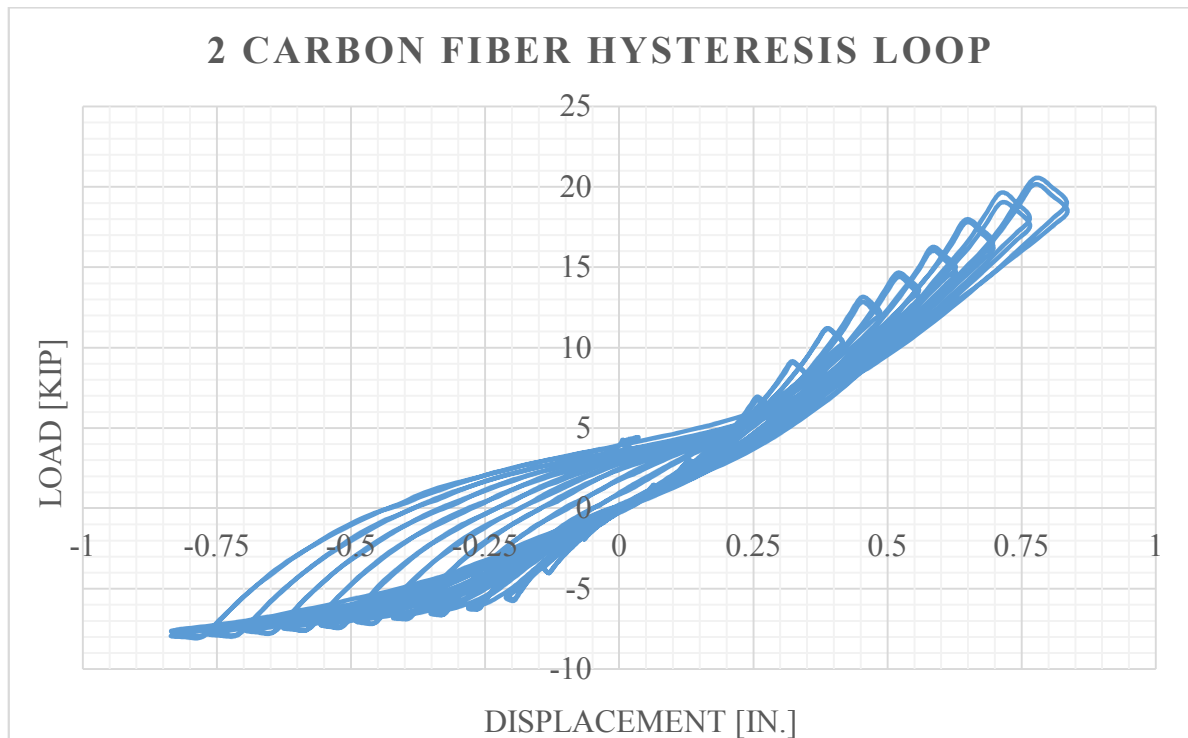


Figure 4-4: 2 CF Hysteresis Curve



Figure 4-5: Beam 2 CF Cracked

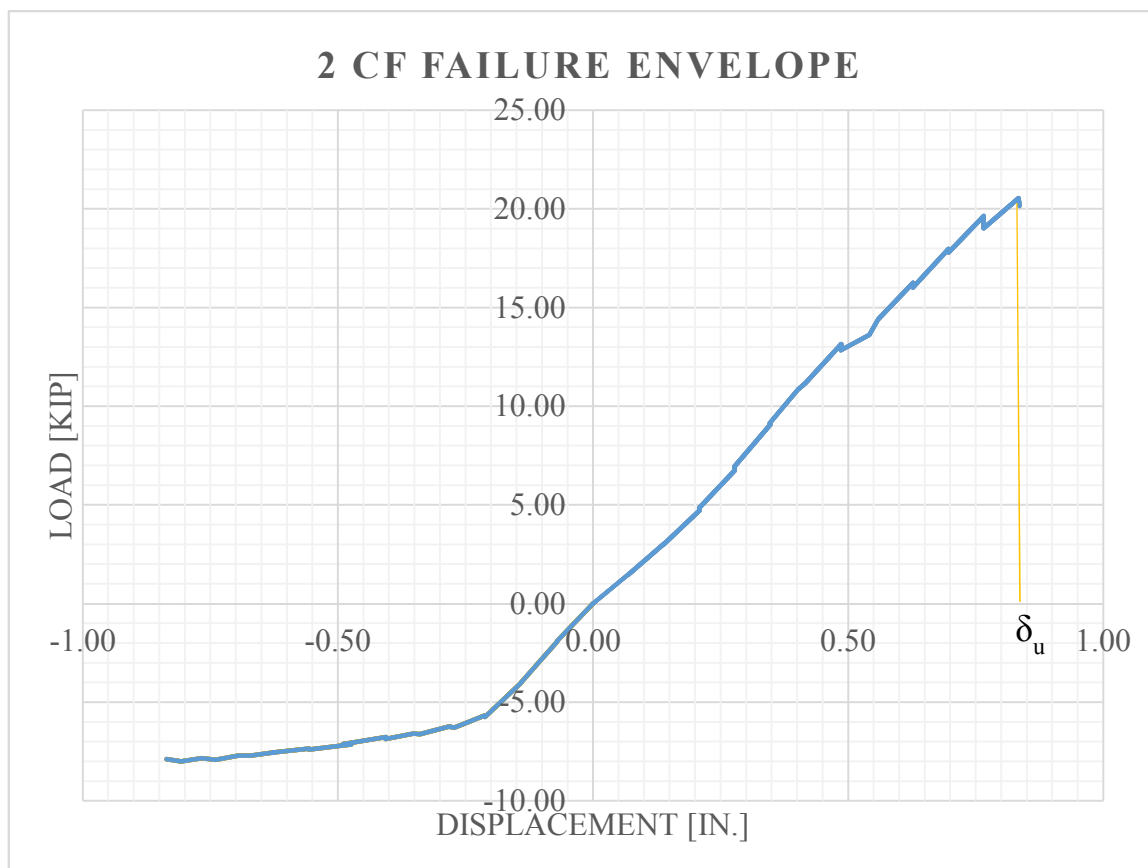


Figure 4-6: 2 CF Failure Envelope

4.2.3 GFRP Reinforced Specimen (3 GF)

Specimen 3 GF had 1 GFRP grid layer as bottom reinforcement of the beam tested under reverse-cyclic loading using a displacement controlled regime. The first crack was observed at a load of 2.5 kips corresponding to a beam mid-span deflection of 0.04 inches in the push direction. The flexural crack occurred almost directly at the mid-span of the beam as shown in Figure 4-6. The cracks were evenly spread out at an average spacing of 8 inches with an average crack width of 0.141 inches. The GFRP delaminated at a load of 8.80 kips corresponding to a GFRP strain value of 0.0336.

As the test continued, the flexural crack at the mid-span of the beam became wider and the GFRP in this region delaminated as the strain in the GFRP exceeded its yield strain. This rupture led to the failure of the sample by flexure as shown in Figure 4-7 and Figure 4-8. The failure envelope for this specimen can be seen in Figure 4-9. The ductility index for this specimen is approximately equal to zero and is also shown in failure envelope, Figure 4-9. As

expected the ductility index for this specimen is nonexistent due to the nature of the brittle GFRP grid material used as reinforcement. Additionally, the shallow slope of the failure envelope indicates a less stiff material in the GFRP grid compared to the steeper slope in the CFRP grid failure envelope, Figure 4-6.

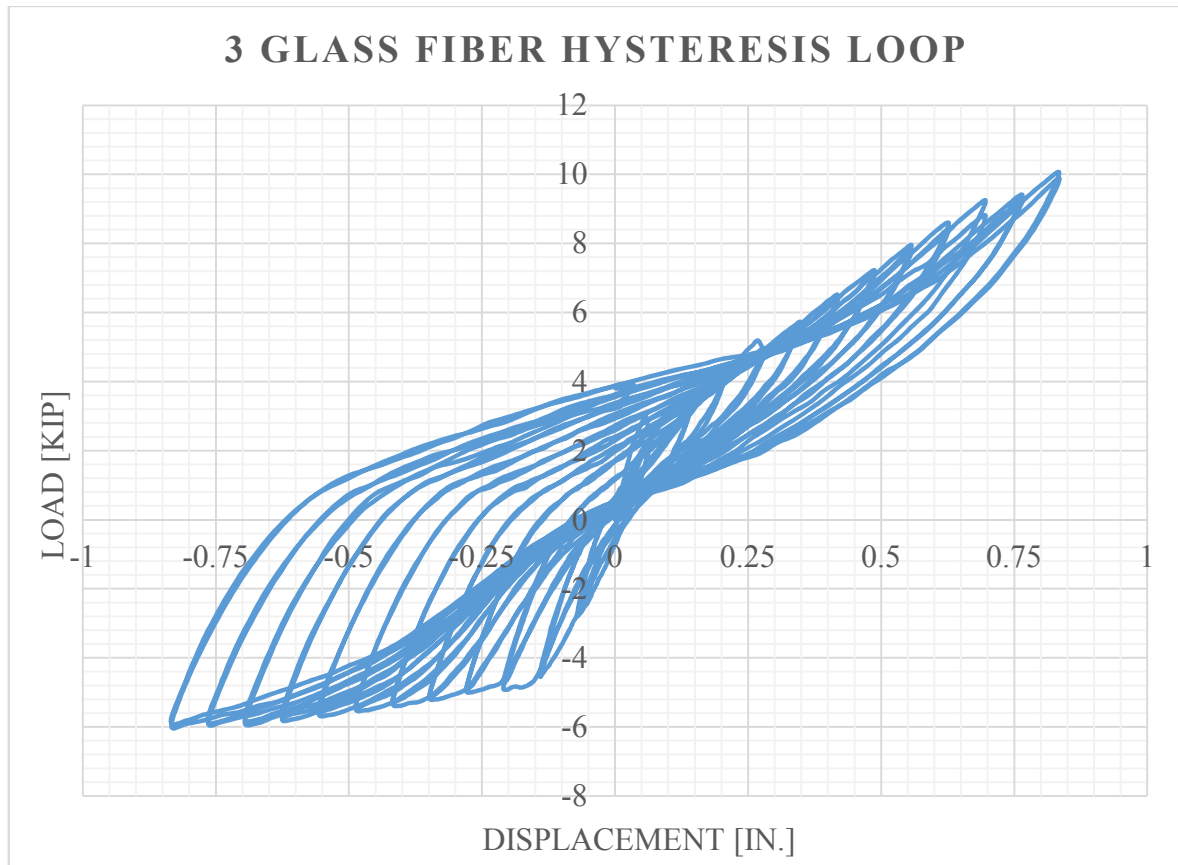


Figure 4-7: 3 GF Hysteresis Curve



Figure 4-8: Beam 3 GF Cracked

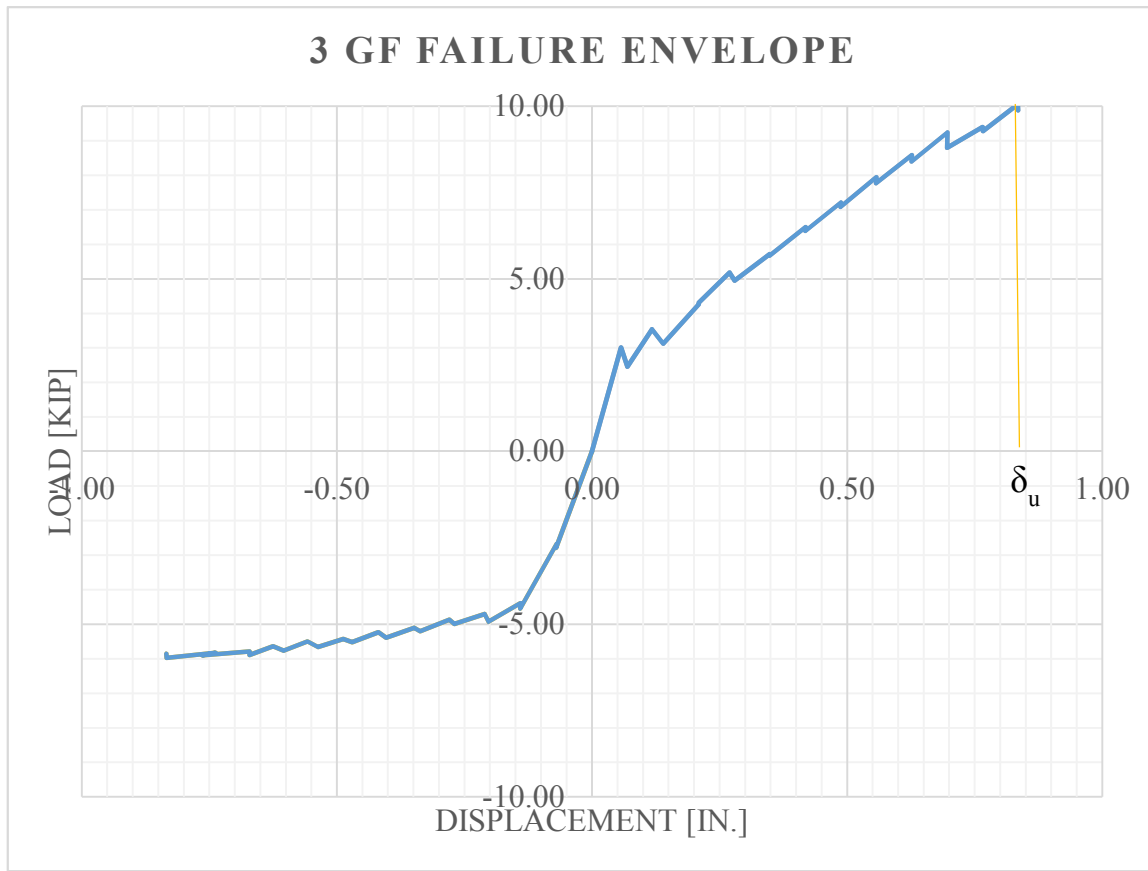


Figure 4-9: 3 GF Failure Envelope

4.2.4 Hybrid Steel and CFRP Reinforced Specimen (4 CF/ST)

Specimen 4 CF/ST had 1 row of CFRP grid with 2 #5 steel bars was used as bottom reinforcement of the beam tested under reverse-cyclic loading using a displacement controlled regime. The first crack was observed at a load of 11.2 kips corresponding to a beam mid-span deflection of 0.206 inches in the push direction. The cracks had an average spacing of 4.6 inches with an average crack width of 0.076 inches. Although there were more cracks observed in this specimen, the crack spacing was lower compared to the 2 CF beam. Additionally, this beam had the smallest average crack width of all beams with the largest being two flexural cracks occurring at the mid-span point of loading vertically downwards with an average crack width of approximately 0.125 inches at failure. Hair line shear cracks can be slightly noticed occurring from the bottom of the beam near the end-supports angled toward the point of loading on top of the beam. However, again the strain in the stirrup did not reach its yield point.

The CFRP delaminated at a load of 24.6 kips before the steel in hybrid connection reached its yield point. The CFRP delaminated at a load corresponding to a CFRP strain value of 0.0336. The CFRP rupture led to a failure of the sample by flexure as shown in Figure 4-10 and Figure 4-11. Soon after the CFRP delaminated, the steel reached its yield point because the load was transferred fully to the steel upon delamination. The steel yielded at a strain value equal to 0.0022 in the first cycle after CFRP delamination, corresponding to a load of 24.9 kips.

Figure 4-12 shows the failure envelope for this specimen. The ductility index for this specimen is approximately equal to 1.94, almost twice beam 2 CF which used only carbon fiber. As expected, the steel in the hybrid reinforcement significantly increased the ductility of the beam.

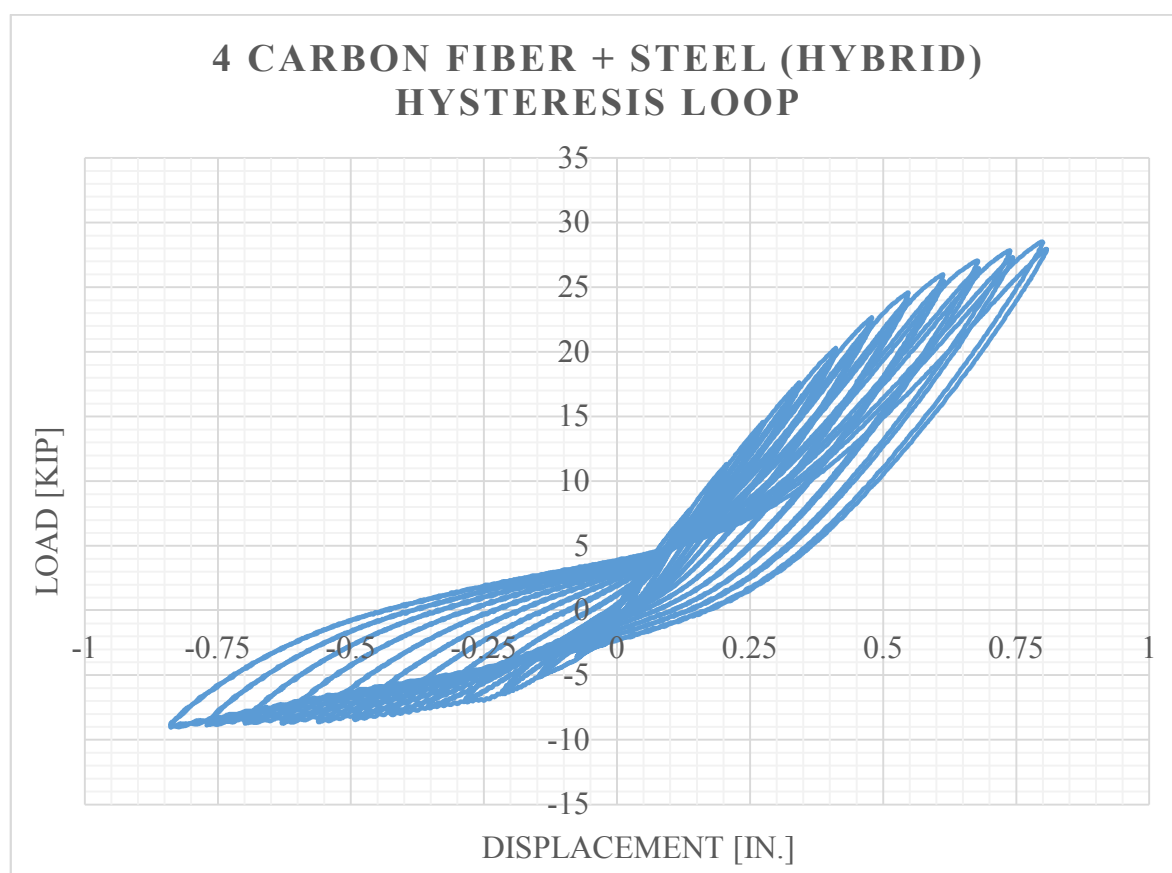


Figure 4-10: 4 CF/ST Hybrid Hysteresis Curve



Figure 4-11: Beam 4 CF/ST Hybrid Cracked

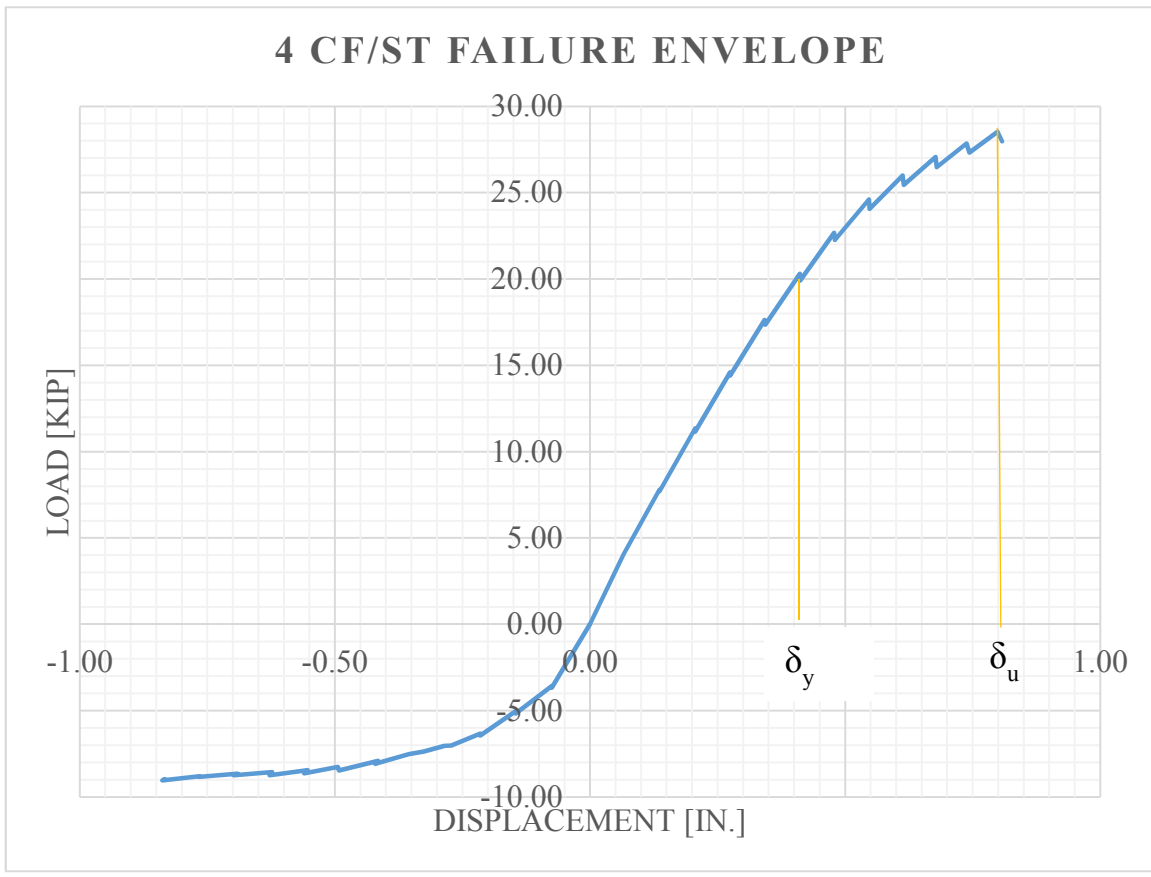


Figure 4-12: 4 CF/ST Failure Envelope

4.2.5 Hybrid Steel and GFRP Reinforced Specimen (5 GF/ST)

Specimen 5 GF/ST had 1 row of GFRP grid with 2 #5 steel bars as bottom reinforcement of the beam tested under reverse-cyclic loading using a displacement controlled regime. The first crack was a flexural crack observed at a load of 7.1 kips corresponding to a beam mid-span deflection of 0.1420 inches in the push direction. The cracks had an average spacing of 4.2 inches with an average crack width of 0.089 inches.

As the test continued the flexural crack occurring at mid-span grew. This crack was the widest crack in the specimen at a width of approximately 0.167 inches. This hybrid GFRP grid beam had a larger number of cracks compared to beam 3 GF; however, the average crack width of this specimen was almost half of the average crack width beam 3 GF. The steel in this specimen yielded first at a strain value of 0.0044 corresponding to a load of 20.3 kips. Soon after the GFRP grid delaminated at a strain value of 0.0338 corresponding to a load of 21.4 kips. The mid-span reinforcement steel yielding and GFRP rupture led to a failure of the sample by flexure as shown in Figure 4-13 and Figure 4-14.

Figure 4-15 shows the failure envelope for this specimen. The ductility index for this specimen is approximately equal to 1.70, much larger compared to beam 3 GF which used only glass fiber. As expected the steel in the hybrid reinforcement increased the ductility of the beam.

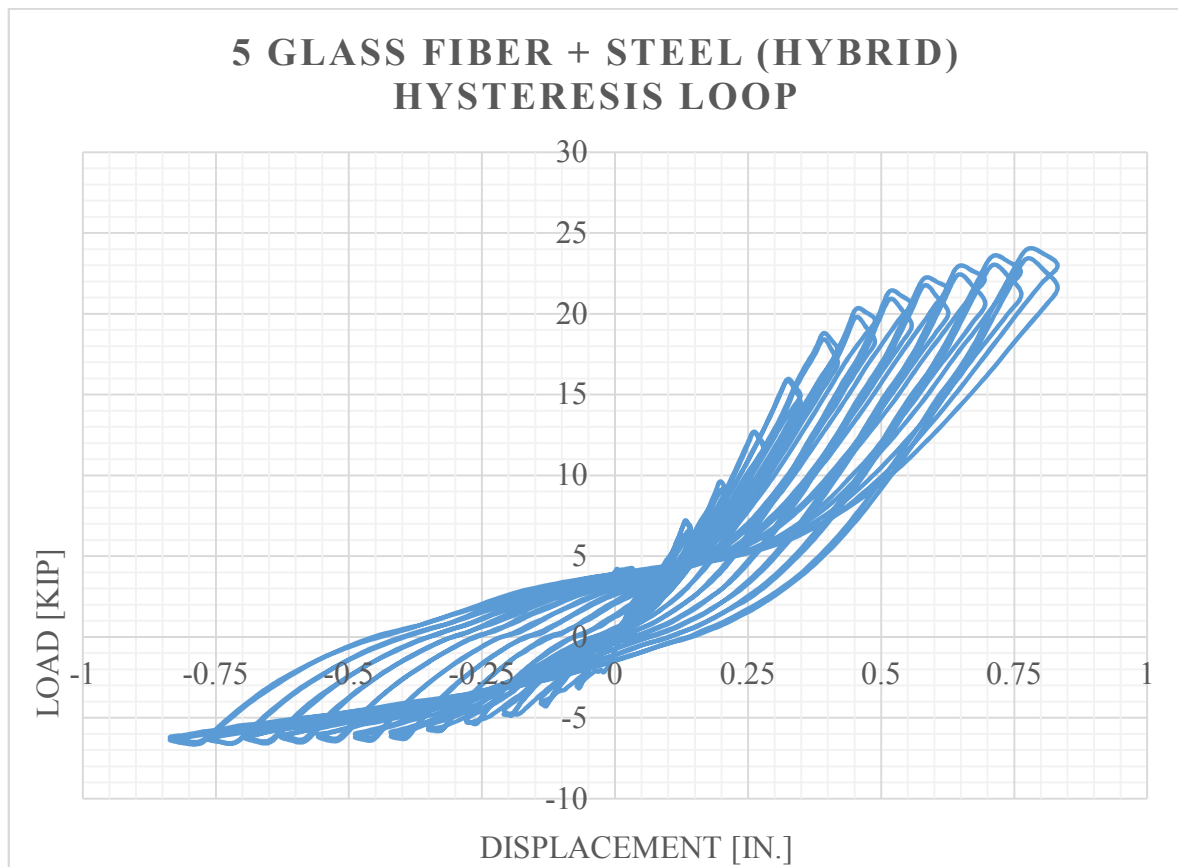


Figure 4-13: 5 GF/ST Hybrid Hysteresis Curve



Figure 4-14: Beam 5 GF/ST Hybrid Cracked

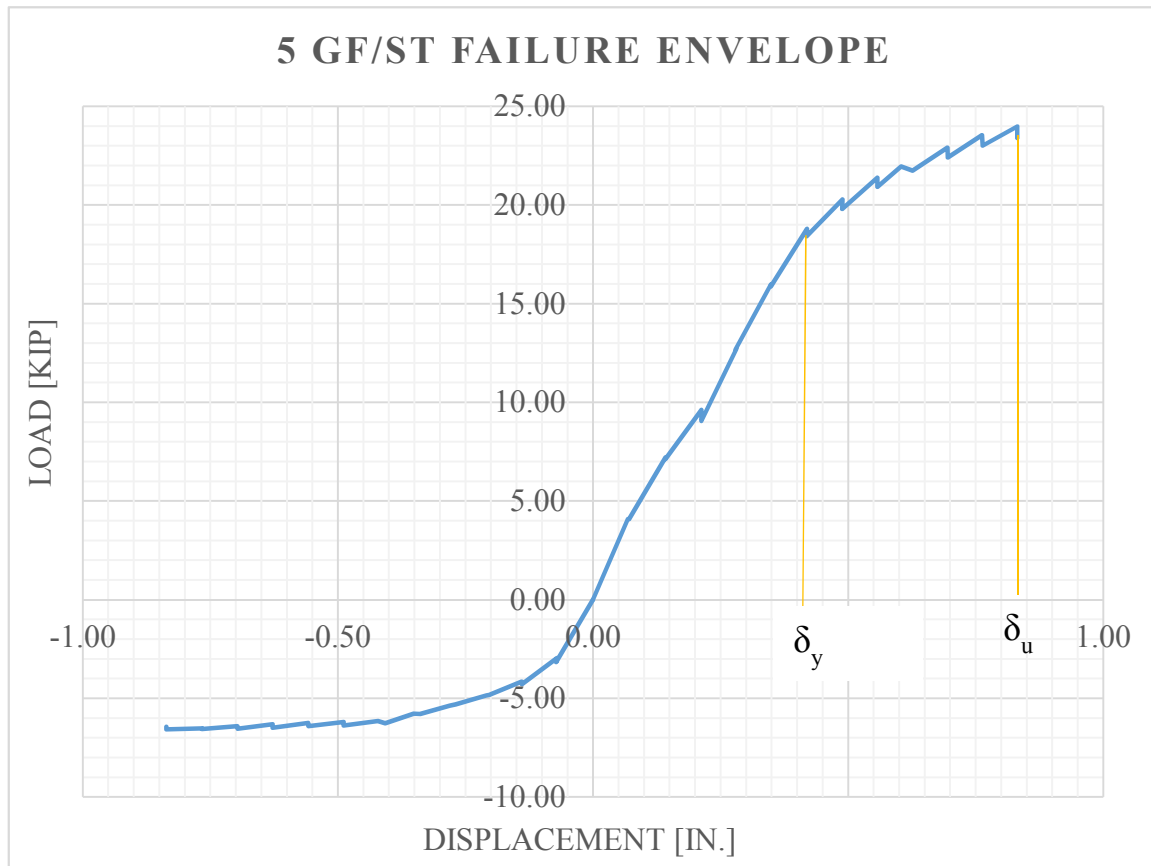


Figure 4-15: 5 GF/ST Failure Envelope

4.3 SUMMARY OF EXPERIMENTAL RESULTS

From the results presented above, it is noted that HSC beams with hybrid reinforcement, specifically FRP grid and steel, have an increase in flexural capacity as well as an increase in ductility. Beams with FRP grids only did not have an increase in flexural capacity. The FRP grid only beams would require additional FRP grids to increase their flexural capacity. The weight of the steel bars used as bottom reinforcement for the control specimen is roughly 7.3 pounds while the carbon fiber and glass fiber grids weigh approximately 3.7 and 2.0 pounds each, respectively. Due to the higher predicted deflections found in the FRP reinforced beams, they are typically service limit state controlled and are designed as over reinforced sections.

Flexural failure was experienced in all beams in this experimental program, which is a local failure and preferable in reinforced concrete structures during seismic action. Table 4-1 and Table 4-2 detail the maximum loads and deflections for all five beams. Table 4-3 shows the maximum strain value for each reinforcement type in all five beams. Correlation between the strain and load data gave yield loads and strains for each beam.

Table 4-4 details the crack width and spacing in all beams. The control beam had the largest crack width; however, it also had the fewest number of cracks. The hybrid sections had the smallest crack widths but had the most amount of cracks. Visual inspection on cracks and the number of cracks can be seen in the results section of each beam individually.

Both of the hybrid reinforced specimens tested showed improved ductility and load carrying capacity as a result of increasing the reinforcement, as shown in Table 4-5. The improved ductility is favored to prevent sudden failure of a concrete section during seismic action. Due to no defined yielding in the FRP reinforced sections their ductility index is taken as zero.

Table 4-1: Summary of Load and Displacement Experimental Results

Specimen	Actuator Load and LVDT Data				Mid-Span LVDT Data	
	Load (Push)	Load (Pull)	Displ. (Push)	Displ. (Pull)	Deflect. (Push)	Deflect. (Pull)
	[kip]	[kip]	[in.]	[in.]	[in.]	[in.]
<i>1 Control</i>	21.00	10.70	0.8246	0.8411	0.6504	0.7231
<i>2 Carbon Fiber</i>	20.60	8.14	0.8356	0.8363	0.7585	0.6323
<i>3 Glass Fiber</i>	10.10	6.11	0.8362	0.8344	0.7178	0.6470
<i>4 CF + Steel</i>	28.54	9.13	0.8081	0.8394	0.7541	0.6294
<i>5 GF + Steel</i>	24.06	6.75	0.8318	0.8366	0.7764	0.7393

Table 4-2: Summary of Experimental Calculations

Specimen	Cracking Load	Ultimate Deflection	Stiffness	Energy Absorption	Failure Mode
	P_{cr} [kips]	δ_u [in.]	[kip/in]	[kip*in]	
<i>1 Control</i>	7.9	0.8411	25.0	13.12	Flexural
<i>2 Carbon Fiber</i>	4	0.8363	24.6	8.96	Flexural
<i>3 Glass Fiber</i>	2.5	0.8362	12.1	5.25	Flexural
<i>4 CF + Steel</i>	11.2	0.8394	34.0	14.52	Flexural
<i>5 GF + Steel</i>	7.1	0.8366	28.8	13.02	Flexural

Table 4-3: Summary of Strain Gauge Experimental Results

Strain Gauge Location	Maximum Strain Value [in./in.]				
	<i>1 CONT</i>	<i>2 CF</i>	<i>3 GF</i>	<i>4 CF/ST</i>	<i>5 GF/ST</i>
Steel	0.03341	N/A	N/A	0.00481	0.00586
CFRP	N/A	0.03570	N/A	0.03373	N/A
GFRP	N/A	N/A	0.03362	N/A	0.03375
Stirrup	0.00077	0.00002	N/A	0.00006	N/A
Concrete	0.03127	0.00002	0.00049	0.00082	0.00022

Table 4-4: Beams Crack Experimental Results

Specimen	Average Crack Spacing [in.]	Average Crack Width [in.]
1 Control	5.7	0.25
2 Carbon Fiber	6.2	0.10
3 Glass Fiber	8.0	0.14
4 CF + Steel	4.6	0.08
5 GF + Steel	4.2	0.09

Table 4-5: Beam Ductility Details

Specimen	Yield Defl.	Ultimate Defl.	Ductility Index
	δ_y [in.]	δ_u [in.]	$\mu = \delta_u / \delta_y$
1 Control	0.277	0.730	2.64
2 Carbon Fiber	N/A	0.834	N/A
3 Glass Fiber	N/A	0.834	N/A
4 CF + Steel	0.411	0.799	1.94
5 GF + Steel	0.489	0.831	1.70

4.4 MECHANISTIC MODEL FOR PREDICTING FLEXURAL CAPACITY OF FRP GRID REINFORCED BEAMS

4.4.1 Introduction

In this chapter, mechanistic models used in predicting the strength of FRP grid reinforced specimens are discussed and analyzed. There have been several studies for concrete beams with external FRP reinforcement. Limited literature is available on internal FRP reinforcement and on hybrid, steel and FRP, reinforcement in high strength concrete beams.

As a result, there are currently no ACI design codes for high strength concrete beams with internal FRP reinforcement. Therefore, the American Concrete Institute's "Building Code Requirements for Structural Concrete, ACI 318-14, was implemented to calculate the expected moment capacities of the beams. With very limited literature available on the design of hybrid, FRP and steel, high strength concrete beams, the prediction of moment capacities

for these beams becomes more difficult. Even though ACI 440R-96 is a state of the art report on FRP Reinforcement for Concrete Structures, no design guidelines are given within the report for internal FRP reinforcement in concrete beams. ACI 440R was used to determine the flexural capacities of the hybrid beams (4 CF/ST and 5 GF/ST.) This section discusses the various mechanistic models used to predict moment capacities, loads, and deflections.

4.4.2 Development of Moment Capacity Models

The moment capacity of beams 1 CONT, 2 CF, and 3 GF were calculated using section analysis as outlined in ACI 318-14. The calculation of the moment capacities of the hybrid beams involved summing the moment capacity provided by the steel and FRP reinforcements, used both ACI 318-14 and ACI 440R methodology.

$$M_n = M_{ns} + M_{nfrp} \quad (\text{Equation 3})$$

In Equation 3, M_{nfrp} is the flexural strength is contributed by the FRP only and M_{ns} is the flexural strength provided by the steel. These moment capacities are calculated using the Equations 4-6 below.

$$M_{nfrp} = T_{frp} * d_{frp} \quad (\text{Equation 4})$$

$$T_{frp} = \varepsilon_{frp} * A_{frp} * E_{frp} \quad (\text{Equation 5})$$

$$A_{frp} = n_{frp} * t_{frp} * b_{frp} \quad (\text{Equation 6})$$

The controlling factor in these calculations is the maximum allowable strain in the FRP reinforcement, ε_{frp} . This value depends on the preferred mode of failure in the FRP reinforced beams. ACI 440R outlines the failure mode into the following groups:

- 1) Concrete crushing in compression before steel yielding.
- 2) Steel yielding in tension followed by rupture of the FRP.
- 3) Steel yielding in tension followed by concrete crushing in compression.
- 4) Delamination of concrete cover in shear or tension.
- 5) Debonding of the FRP from the concrete.

Figure 4-16 details the moment capacity relationship between an FRP reinforced concrete beam and a traditional steel reinforced beam. Due to the brittle properties of the FRP material,

the sudden failure of FRP reinforced concrete specimens must be avoided. Thus, the debonding of the FRP from the concrete due to the epoxy delamination is assumed to limit the moment capacity.

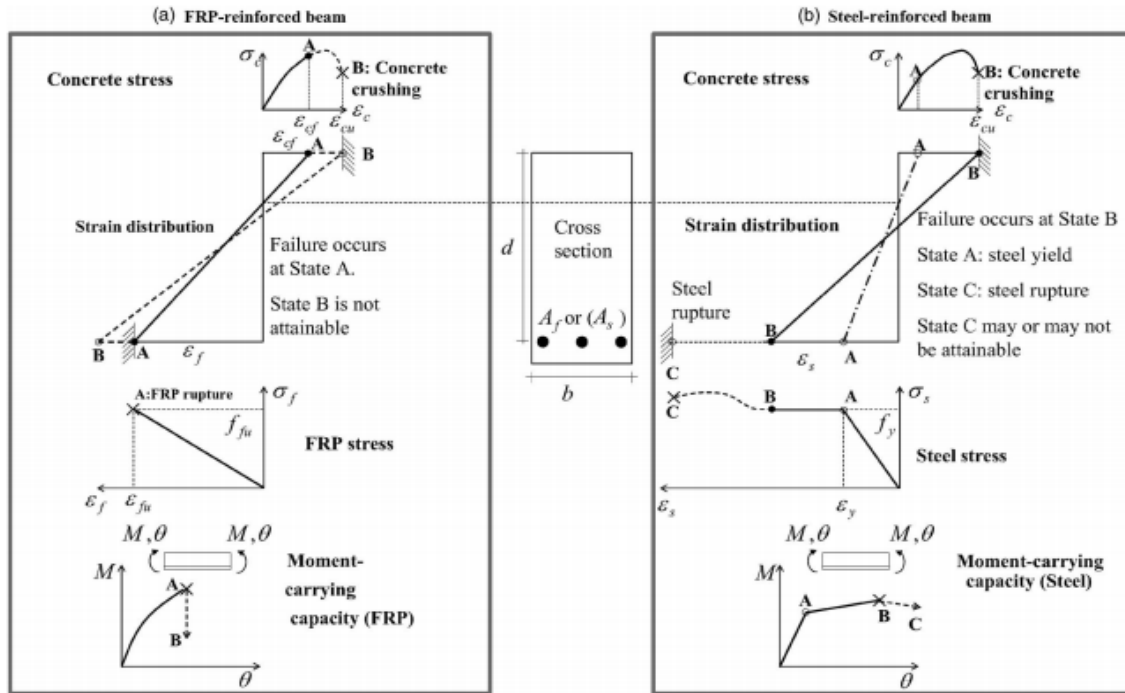


Figure 4-16: Stress-Strain Relationship in FRP and Steel Reinforced Beams

For one of the experimental procedures in this section, the maximum allowable strain in the FRP is limited to the strain at which debonding will occur. This value is then used to calculate the tensile strength of the FRP material in Equation 5 for section analysis. The stress-block for the beams with FRP reinforcement only, while neglecting the top reinforcement, is shown in Figure 4-17. For the hybrid beams, A_f has two components: steel and FRP.

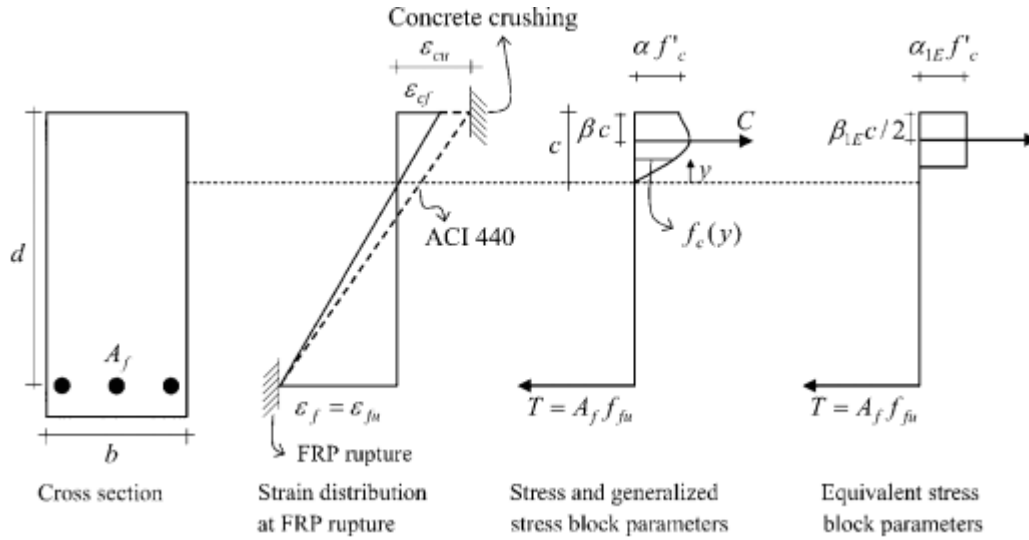


Figure 4-17: Stress Block Diagram for Section Analysis

From Figure 4-17, Equation 7 is applied to maintain section equilibrium. Neglecting the top reinforcement for all beams generates, T , the tensile force, and C , the compressive force, into Equations 8 and 9 below. In these equations, α is taken as 1.25 to account for strain hardening and α_1 as 0.65 based on the strength of the concrete.

$$C = T_s + T_{frp} \quad (\text{Equation 7})$$

$$C = \alpha_1 * f'_c * A_c \quad (\text{Equation 8})$$

$$T_s = \alpha * f_y * A_s \quad (\text{Equation 9})$$

In order to solve equations 7 and 9 using section equilibrium, the strain in the FRP is taken as debonding strain from experimental results.

The last two moment capacity models used ACI 318-14 and the FRP tensile strength as recommended in ACI 440R. The first model used the given FRP material tensile strength and the second model used 60% of the given FRP tensile strength as recommended in ACI 440R. The last model using 60% of the tensile strength provided the most accurate results compared to the experimental values. Equation 10 is obtained from section equilibrium and solves for the depth of the equivalent rectangular stress block. Equation 11 solves for the recommended yield tensile strength of the FRP material used in Equation 12 to solve for the beam factored nominal moment capacity.

$$a = \frac{A_s * f_y}{0.85 f'_c * b} \quad (\text{Equation 10})$$

$$f_{yfrp} = 0.6 * f_{uFRP} \quad (\text{Equation 11})$$

$$M_n = 0.85 f_{yfrp} * A_{frp} \left\{ d - \frac{a}{2} \right\} \quad (\text{Equation 12})$$

Table 4-6 shows the calculated moment capacities for all three models discussed in this section compared to the experimental results from the reverse-cyclic analysis on all five beams.

Table 4-6: Experimental and Mechanistic Models Moment Capacities

Code Used:	Experimental	ACI 318-14 (Material Properties)	ACI 318-14 (60% FRP strength)	ACI 440R
Specimen	ϕM_n	ϕM_n	ϕM_n	ϕM_n
	[kip*ft]	[kip*ft]	[kip*ft]	[kip*ft]
<i>1 Control</i>	21.48	22.7	N/A	N/A
<i>2 Carbon Fiber</i>	18.03	30.5	18.7	N/A
<i>3 Glass Fiber</i>	8.84	12.4	7.5	N/A
<i>4 CF + Steel</i>	24.97	49.3	40.0	43.2
<i>5 GF + Steel</i>	21.05	32.8	28.6	33.2

4.4.3 Development of Deflection Capacity Model

The development of deflection capacities used two primary equations:

$$I_{cr} = \frac{b * c_{cr}^3}{3} + n * A_R (d - c_{cr})^2 \quad (\text{Equation 13})$$

$$\delta_u = \frac{P * L^3}{192 * E * I_{cr}} \quad (\text{Equation 14})$$

Equation 14 is the mid-span deflection of a beam that is fixed at both ends, as in the case of this experimental program. Equation 13 is the cracked moment of inertia for each beam based on the beam width, b , cracked depth of compression block, c_{cr} , modular ratio, n , area of reinforcement, A_R , and depth of beam to bottom reinforcement, d . The calculation for these

variables can be seen in Table 4-7. As this was a displacement controlled reverse-cyclic test and all beams were tested at the same loading protocol, the mid-span deflections obtained from the LVDT are very similar to one another. As expected the mechanistic model predicts larger deflections in the FRP reinforced beams due to the low modulus of elasticity of those beams. Conversely, the steel in the hybrid beams reduced their deflections.

Table 4-7: Mechanistic Model Deflections

Specimen	Equation 10/11 Defl.		LVDT Mid-Span	LVDT Mid-Span
	δ_y	δ_u	Deflection (Push)	Deflection (Pull)
	[in.]	[in.]	[in.]	[in.]
1 Control	0.065	0.088	0.8246	0.8411
2 Carbon Fiber	0.263	0.428	0.8356	0.8363
3 Glass Fiber	0.472	0.781	0.8362	0.8344
4 CF + Steel	0.191	0.244	0.8081	0.8394
5 GF + Steel	0.18	0.205	0.8318	0.8366

4.4.4 Development of Ductility Model

The ductility index for each beam was calculated using Equation 12. This same equation was used to calculate the experimental ductility index values. Although the ductility index values obtained from experimental testing are different than the mechanistic model calculations, the beams follow the same pattern, i.e. 1 CONT was the largest and 5 GF/ST was the smallest.

Table 4-8: Ductility Calculations

Specimen	Experimental	Mechanistic Model
	μ	μ
1 Control	2.64	1.52
2 Carbon Fiber	N/A	N/A
3 Glass Fiber	N/A	N/A
4 CF + Steel	1.94	1.28
5 GF + Steel	1.70	1.14

4.4.5 Summary of Mechanistic Models

In summary ACI 318-14 and ACI 440R were used to calculate moment capacities, crack width and deflections for the beams. Table 4-9 compares the mechanistic values to the data obtained during experimental testing. The hybrid beams showed the most variation due to limited resources available on behavior of hybrid FRP and steel reinforced concrete beams.

Table 4-9: Mechanistic Model Values versus Experimental Data

Code Used:	$\frac{M_{nACI 318 (fy)}}{M_{nEXPERIMENT}}$	$\frac{M_{nACI 318 (0.6fy)}}{M_{nEXPERIMENT}}$	$\frac{M_{nACI 440}}{M_{nEXPERIMENT}}$	$\frac{M_{ACI 318 (0.6fy)}}{M_{EXPERIMENT}}$
Specimen				
<i>1 Control</i>	1.06	1.06	N/A	0.58
<i>2 Carbon Fiber</i>	1.69	1.04	N/A	N/A
<i>3 Glass Fiber</i>	1.41	0.85	N/A	N/A
<i>4 CF + Steel</i>	1.97	1.6	1.73	0.66
<i>5 GF + Steel</i>	1.56	1.37	1.58	0.67

CHAPTER 5: SUMMARY AND CONCLUSIONS

The main goal of this study is to investigate the behavior of high strength concrete beams with varying steel, FRP, and hybrid reinforcement under reverse-cyclic loading. For this experimental program, five high strength concrete beams were prepared and cast using a concrete with compressive strength of 8.5 ksi. All beams produced were 7 feet long, 9 inches in depth and 8 inches wide. The control beam was reinforced with Grade 60 #5 steel bars and others were reinforced with carbon fiber and glass fiber grids. Additionally, the last two beams were reinforced with steel and FRP. All beams used 2#3 Grade 60 steel rebar for top reinforcement and as stirrups spaced at 8 inches. The beams were fixed on both ends and subjected to a three-point displacement controlled reverse-cyclic loading. A 50 kip maximum servo-value hydraulic actuator was used to perform this test.

The data collected in this study included the following: load-displacement (mid-span), strain in FRP grids, steel rebar, stirrups, and concrete, mode of failure and crack spacing and thickness. The experimental results are compared to mechanistic models from the literature found. Limited data is provided in the literature on behavior of similarly reinforced concrete beams. The mechanistic models predict moment capacity for each beam depending on tensile stress of the reinforcement used. Additionally, the models predict yield and ultimate deflections.

The study concluded that the behavior of the HSC beams was primarily dependent on the tensile strength and modulus of elasticity of each type of reinforcement. The moment capacity calculations using code ACI 318 and 60% of the given tensile strength as provided in ACI 440R were in good agreement with the experimental results. For the hybrid reinforced beams, moment capacities calculated using ACI 440R were over-estimated. Although ACI 440R assumes externally wrapped FRP, the sectional analysis was performed the same way as ACI 318. The yield and ultimate deflection calculations using ACI 318 and 60% tensile strength were proven to be under-estimated; primarily due to the displacement controlled test.

The following conclusions were reached after the experimental and mechanistic study:

- It is feasible to use CFRP and GFRP grids as reinforcement in high strength concrete beams.

- It is practicable to use a hybrid, steel and CFRP/GFRP grids as reinforcement in high strength concrete beams.
- Beams 2 CF and 3 GF showed improved strength degradation compared to Beam 1 CONT. This is shown by the stiffness increasing as the test progressed in the FRP only reinforced beams.
- The hybrid reinforced beams showed an increase in moment capacity and ductility for both the CFRP and GFRP beams. The moment capacity increase ranges from 138% - 238% compared to the moment capacity of FRP only reinforced beams. The ductility index increase capacity ranges from 170% - 194% due to no yield point provided in the FRP only reinforced beams.
- The hybrid beams (4 CF/ST and 5 GF/ST) had an increase in moment capacity compared to the control beam (1 CONT) due to the FRP grid delaminating before the steel strain yielded in the same loading cycle.
- Under-reinforced FRP beams showed a decrease in moment capacity compared to the Grade 60 #5 steel rebar control beam. The decrease in capacity was 98% for the CFRP reinforced beam and 48% for the GFRP reinforced beam.
- The hybrid reinforced beams had a larger number of cracks but with an average crack spacing of approximately 75% and 88% of the corresponding FRP reinforced only cracks for beams 4 CF/ST and 5 GF/ST, respectively.
- The model results using ACI 318 and 60% of the FRP tensile strength from ACI 440 showed relatively good agreement with the experimental results.
- Model calculations using ACI 440R over-estimates the moment capacity for the hybrid reinforced beams due to it being specifically for externally wrapped FRP concrete beams.
- Deflection prediction calculations using 60% FRP tensile strength and ACI 318 were underestimated by 25% - 88%. Although, the predicted deflections did follow the same ranking order from Beam 1-5 as the experimental values.
- Ductility predictions using ACI 318 were under-estimated by 58% - 67% largely because the test was displacement controlled. In both the experimental and predicted value, beams 1 CONT and 4 CF/ST had the largest and smallest ductility index values, respectively.

REFERENCES

- [1] Aroumugame, A. P. (2016). Comprehensive Study of High Strength Concrete Beams with Confinement Shear Reinforcement under Cyclic Loads. *International Journal of ChemTech Research*, 1-11. Retrieved January 10, 2018.
- [2] Ashtiani, M. S. (2012). Cyclic Beam Bending Test for Assessment of Bond-Slip Behavior . *WCEE 15*,1-9.
- [3] Badogiannis, E., & Kotsovos, M. (2014). Monotonic and cyclic flexural tests on lightweight aggregate concrete beams. *Earthquakes and Structures*, 6(3), 317-334. doi:10.12989/eas.2014.6.3.317
- [4] Bakis, C. E., Bradberry, T. E., Nanni, A., & Shield, C. (2006). Guide for the Design and Construction of Structural Concrete Reinforced with FRP Bars (Rep. No. ACI 440.1R-06).
- [5] Berg, A. C. (2005). Construction and Building Materials. Construction and cost analysis of an FRP reinforced concrete bridge deck, 20(515–526), 1-12.
- [6] Bisby, L. A. (2006). Application and Handling of FRP Reinforcements for Concrete (Educational Module 6). ISIS Canada.
- [7] Cyclic/Fatigue Loading of Structural Members. (n.d.). Retrieved from <http://wiredspace.wits.ac.za/bitstream/handle/10539/4714/CHAPTER%202.pdf;jsessionid=600AFC6271B748EEE8CF1CEDDBF6165D?sequence=2>
- [8] Dong, J. F. (2012). Structural behaviour of RC beams externally strengthened with FRP sheets under fatigue and monotonic loading. *Engineering Structures*, 1-10.
- [9] Fang I-Kuang, Yen Shih-Tzung, Wang Chwen-Shyuan, Hong Keh-Luen. Cyclic behavior of moderately deep HSC beams. *ASCE, Journal of Structural Engineering* 1993; 119(9).
- [10] Fang I-Kuang, Wang Chuen-Shyuan, Hong Keh-Luen. Cyclic behavior of high-strength concrete short beams with low amount of flexural reinforcement. *ACI Structural Journal* 1994; 91(1):10–8

- [11] FRP Reinforcement Engineering. (n.d.). Retrieved November 13, 2017, from <http://www.build-on-prince.com/frp-reinforcement.html>
- [12] Kara, I. F. (2015). Flexural behavior of hybrid FRP/steel reinforced concrete beams. *Composite Structures*, 1-11.
- [13] Klemens, T. (2005, January 1). Specifying concrete for performance: always a gamble, your best bet might be to seek expert advice. *Concrete Construction*.
- [14] Narendran, L. (2013). Cost Estimation of Fiber Reinforced Polymer (FRP) Repairs on Rail and Highway Bridges. *WVU Scholar*, 1-95.
- [15] Oehlers, D. J., Ali, M. S., Haskett, M., Lucas, W., Muhamad, R., & Visintin, P. (2011). FRP-Reinforced Concrete Beams: Unified Approach Based on IC Theory. *Journal of Composites for Construction*, 15(3), 293-303. doi:10.1061/(asce)cc.1943-5614.0000173
- [16] Peng, G., Zhang, J., & Hao, T. (Eds.). (2014). High performance concrete - innovation & utilization : selected, peer reviewed papers from the 10th international symposium on high performance concrete - innovation & utilization (hpc 2014), September 16-18, 2014, Beijing, China. Retrieved from <https://ebookcentral.proquest.com>
- [17] Qureshi, M., Tandel, Y., & Patel, B. (2013). An Experimental Study On High Strength Concrete Using Fly Ash And Alccofine. *I-Manager's Journal on Structural Engineering*, 2(4), 1-9.
- [18] Rajkumar, K., & Vasumathi, A. (2012). Flexural Behavior of Fiber Reinforced Concrete Beams Confined with FRP. *Applied Mechanics and Materials*, 256-259, 938-941. doi:10.4028/www.scientific.net/amm.256-259.938
- [19] Servo Hydraulic Test Machines for Durability, Fatigue, Vibration | Shore Western. (n.d.). Retrieved September 15, 2017, from <http://www.shorewestern.com/>
- [20] Sharbatdar, M. K. (2008). Monotonic and cyclic loading of new FRP reinforced concrete cantilever beams. *IJCE*, 1-14.

- [21] Strengthening of Concrete Structures Using FRP Composites. (n.d.). Retrieved January 11, 2018, from <http://www.structuremag.org/?p=8643>
- [22] Wang, Y. C. (2006). Experimental study of FRP-strengthened RC bridge girders subjected to fatigue loading. *Composite Structures*, 1-8.
- [23] West, J. S. (2011). An Introduction to FRP-Reinforced Concrete (Educational Module 3). ISIS Canada.
- [24] Xiao Yan, Ma Rui. Seismic behavior of high strength concrete beams. *The Structural Design of Tall Buildings* 1998; 7:73–90.
- [25] Xue, W. (2007). The reversed cyclic load tests of normal and pre-stressed concrete beams. *Engineering Structures*, 30, 1-10.
- [26] Yost, J. R. and Schmeckpeper, E.R., (2001). “Flexural Behavior of Concrete Beams Reinforced with FRP Grids”. *Journal of Composites for Construction*, Vol. 5, No. 1, pp. 18-25.

APPENDICES

APPENDIX-A: SHORE WESTERN CONTROLLER SYSTEM INTRODUCTORY MODULE

A.1 BACKGROUND

According to the Shore Western website, [19], this controller system “is an industry-leading customizable servo hydraulic PID controller with command optimization.” This section discusses the powering, operation, and test running of the SWCS located in BEL at the UI. The SWCS controls the hydraulic actuator used for this experimental program. The hydraulic actuator located in BEL has a cylindrical motor that uses hydraulic power to generate mechanical operation. Inside the cylindrical motor is a hollow tube along which a piston slides and any change in pressure between the two sides of the piston moves the piston from one side to the other. This piston movement attached to a load cell with an internal LVDT is attached to a gyro-rotational clevis meant to withstand any load produced by the actuator. This clevis is then fixed to or pressed against a specimen to run various strength tests.

The hydraulic actuator used in BEL has a load cell (50 kip maximum). Additionally, there is an internal LVDT located within the piston that measures displacement along the piston shaft, in both directions. The load and displacement are recorded and displayed by the SWCS for each test completed.

A.2 SYSTEM STARTUP

The startup routine to power the hydraulic system and to complete tests using the SWCS is a two-part method. The first involves preparing BEL 125 for safe testing and machine power up. The second deals with the computer power up and how to properly use the SWCS software. The following tasks must be completed in the order as listed below to successfully startup the actuator and controller system:

- 1) Turn the yellow pump coolant water valve to the open position, as shown circled in Figure A-1. The valve system is located in the northwest corner of BEL 125.

- 2) Both pumps must be powered on to properly use the primary pump (Shore Western Pump) for this system. Turn on power to both the pumps as shown in Figure A-2. The pump power boxes are located on the west wall of BEL 125.
- 3) After the Shore Western Pump has been powered on the “Over Temp Error” button will light up as shown in Figure A-3. Push the lit up button to activate automatic shutoff if the pump overheats.
- 4) Ensure the red Emergency Stop button is pulled out as shown in Figure A-4. This button may be pushed to automatically turn power to the pump off in the event of an emergency.



Figure A-1: Pump Coolant Water Valve Open



Figure A-2: Pump Power Switches On



Figure A-3: Shore Western Pump Display



Figure A-4: Shore Western Pump Emergency Stop Button

The machines used for testing are now powered on and ready to use. The next set of steps are to be completed on the computer with the SWCS software.

- 1) Turn on the power to the computer next to the pump by pushing the button on the front tower box.
- 2) Click on the desktop application titled “Start SW” to open the SWCS software. Upon startup of the SWCS Application located on the desktop of the computer in BEL 125 Figure A-5 is displayed.
- 3) Next, the “System Startup” button may be pressed. A system startup subroutine was developed using the block programming in the SWCS. Follow the steps in the series of dialog boxes appearing once this button is pressed. The first dialog box is shown in Figure A-6.
- 4) Twist the E-Stop button to the off position and push the lit up button in front of it to activate the emergency stop feature remotely from the computer system.

- 5) Push yes to both dialog boxes asking to turn the pump to low pressure and then high pressure. In high pressure the pump should run near 2300 psi. The Shore Western Pump pressure gauge is shown in Figure A-7.
- 6) The system is now successfully on and safe tests may be run.



Figure A-5: SWCS Default Startup Homepage

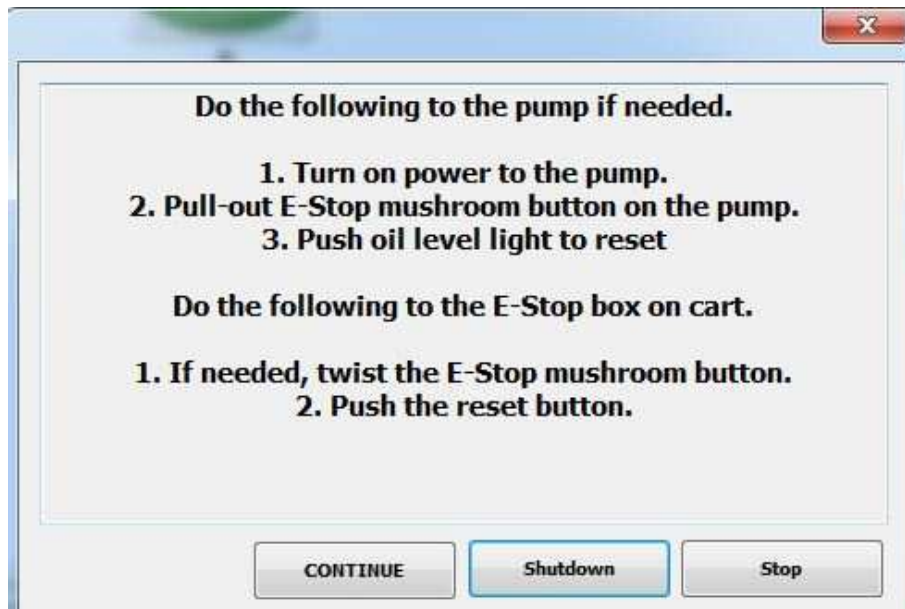


Figure A-6: System Startup Routine Display



Figure A-7: Shore Western Pump Pressure Gauge

A.3 TEST SET UP

Once the system is successfully started, the system will operate in displacement control to maintain stroke length and not damage any equipment. The system may be used in displacement or load control. In load control the actuator piston will stroke its entire length to provide the desired load. This actuator piston has roughly a 7 inch stroke. Displacement control testing is typically much safer because the actuator will extend or shorten to the desired input displacement and stop, rather than continue to full/closed stroke. The user may switch between displacement and load control by clicking on the desired button shown in the “All in One” panel displayed in Figure A-5.

As mentioned previously, these buttons were developed by SWCS software engineers as subroutines. To manually override the buttons and control pressure level or power the “System Tree” can be opened clicking on the bold “T” located at the top left of the screen near the panel display buttons, shown in Figure A-8. The green box indicates which panel is active in

the main viewing screen. Clicking the plus sign with no green makes all 4 working directory panels available in the main viewing screen.

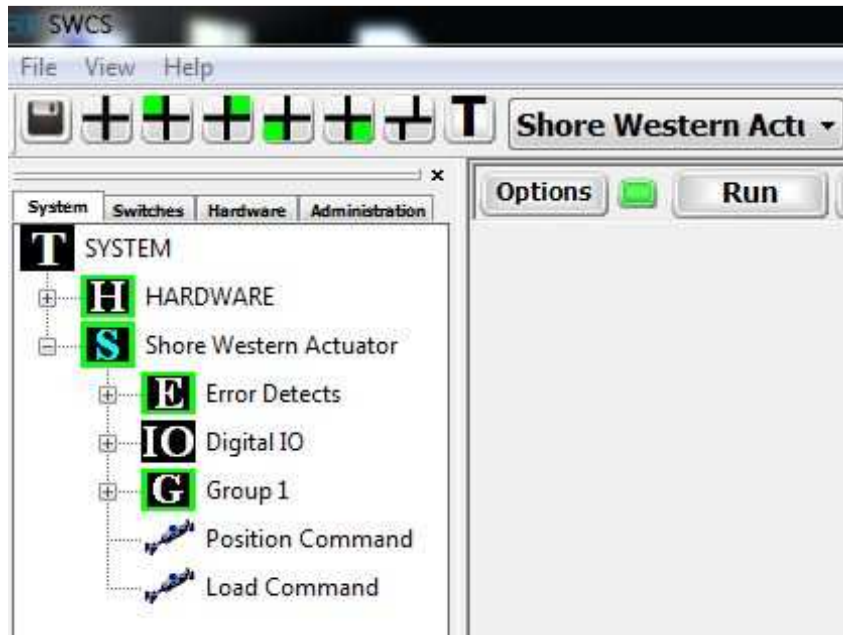


Figure A-8: SWCS Hardware Tree System

Once a specimen is loaded and the test protocol has been established, the user should tare the load and displacement to zero by clicking the tare button below the value indicator as shown in Figure A-9. Next, a test may be selected from the dropdown menu titled “Reverse Cyclic Displ Control” in Figure 4-5. SWCS customer service has developed various tests and preloaded them onto the computer software. Some examples of tests already loaded onto the computer are: fatigue testing displacement/load controlled, monotonic testing displacement/load controlled, and reverse-cyclic displacement/load controlled.

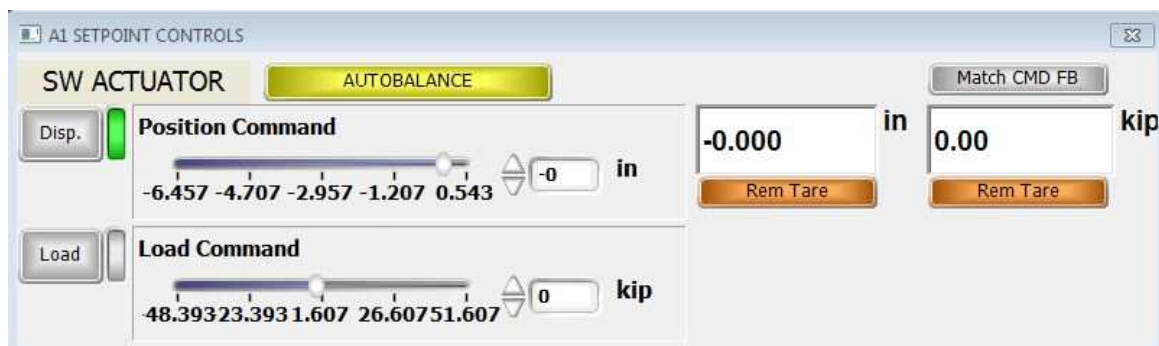


Figure A-9: Test Setup to Tare Displacement and Load Values

After the test has been designated and the loading protocol is chosen, the settings and parameters for each test will need to be set within the test settings. Figure A-10 is an example of a monotonic displacement control test. The user may input the correct parameters and run the test to record the correct the data.

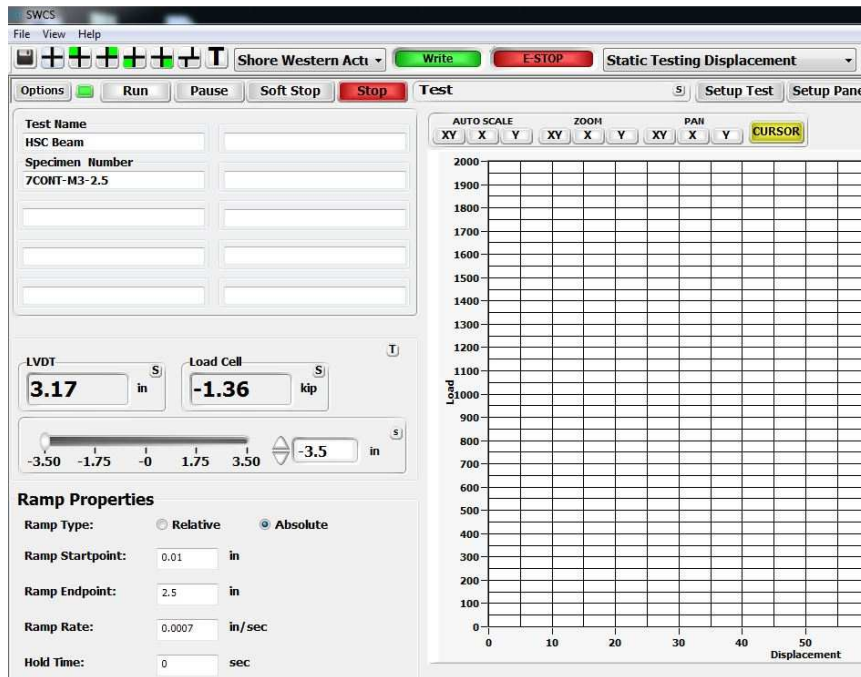


Figure A-10: Monotonic Displacement Control Test SWCS Home Screen

For a fatigue or reverse-cyclic test, the parameters are much more user extensive. The function chosen for the test will dictate which settings needs to be controlled. Figure A-11 displays the home screen for a displacement controlled reverse-cyclic test, the same test used for this research. The dropdown menu below Function Generator has various types of functions (i.e. sine wave, triangle wave, saw-tooth wave, time-history function, etc.) that may be used for testing. Once the function is selected the loading protocol may be applied to the system.

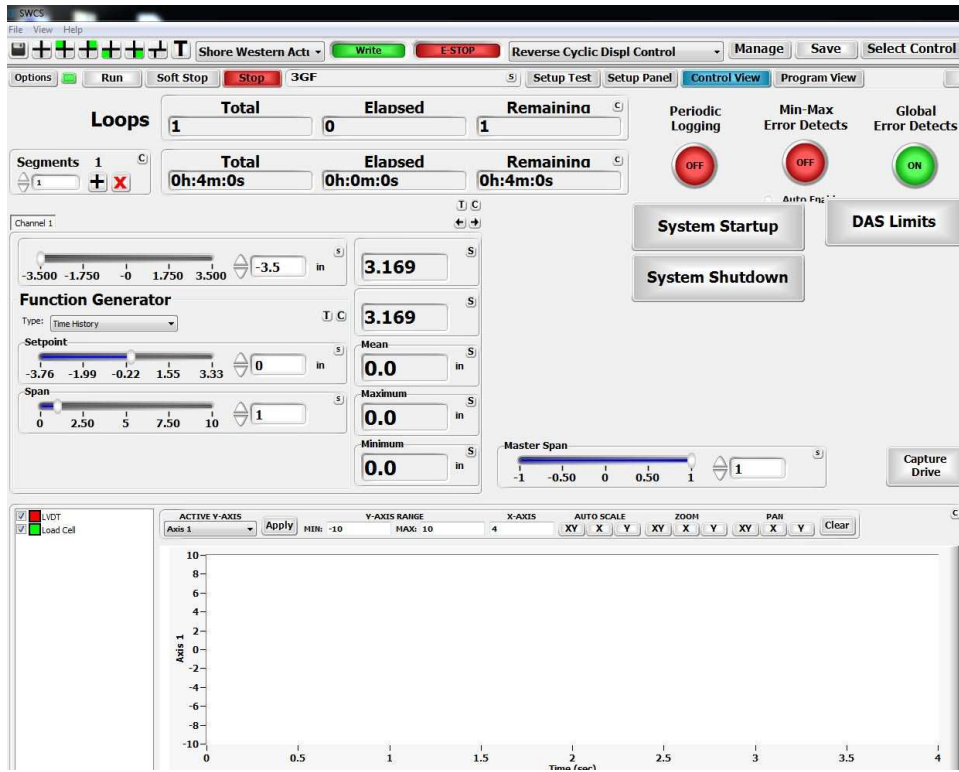


Figure A-11: Reverse-Cyclic Displacement Control SWCS Home Screen

Figure A-12 and Figure A-13 display all the parameters input for this experiment. SWCS prides themselves on being an independent program allowing users to program each test to the specific needs required, without unnecessary information being recorded for each test. For further information on the Shore Western Controller System and its applications see the user manual found online or contact the company directly.

Channel Parameters

Name: Channel 1

Control Type: RTAC

Soft Start Stop

Start
 Enabled
 Duration: 5 sec

Stop
 Enabled
 Duration: 5 sec

Command

Cycles Per Loop: 1

Reset Drive On Loop

Show Command Plot

Base Line Correction
 Enable Cycles Per Update: 1

Enable Drive Limits
 Lower Limit: -3.7633 in
 Upper Limit: 3.4126 in

Min/Max Error Detects

Enable
 Error Band: 5 % of Value

Use Minimum Error Band
 Minimum Band: 0

Trip Count: 10

Absolute Error Detects

Enable
 Absolute Min: 0
 Absolute Max: 0

Trip Count: 1

Ramp To Setpoint

Enabled

Feedback Channel: LVDT

Ramp Properties

Ramp Type: x-sinx

Ramp Time: 2 sec

Acceptable Error: 0.05 in

Persistence: 100

Filter
 Filter Enabled
 Window Size: 5

Jacobian
 Use Compensation
 Gain Range: 0 dB

Proportional Gain
 Gain Range: -2 dB

Integrator Gain
 Gain Range: 0 dB

Rate Gain
 Gain Range: 0 dB

Figure A-12: Time-History Function Channel Parameters

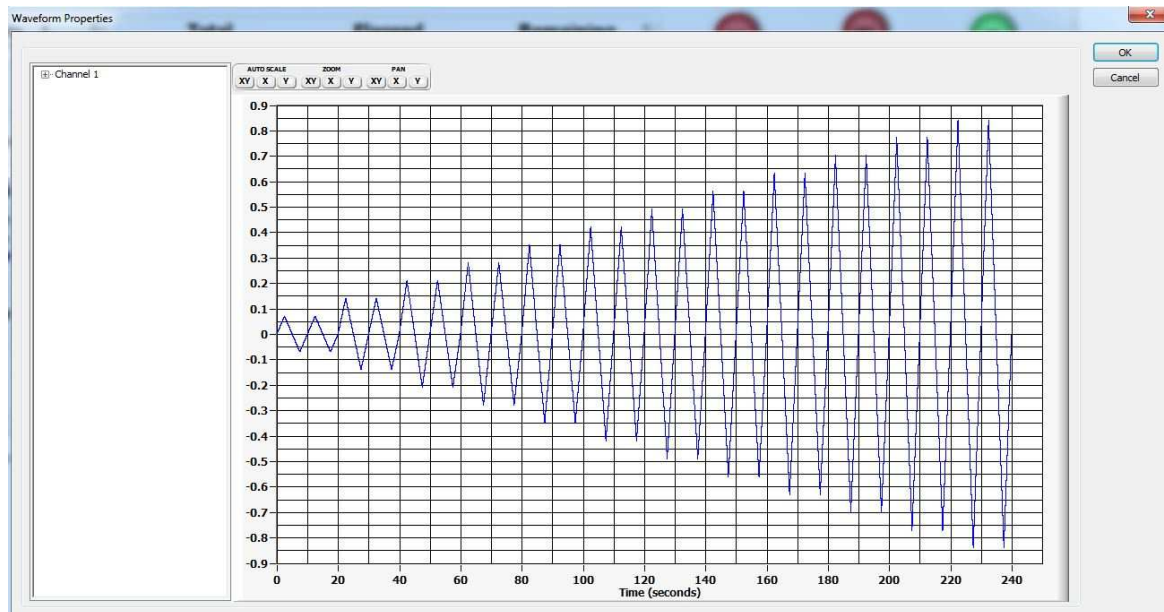


Figure A-13: Waveform Properties for a Time-History Function


A.4 SYSTEM SHUTDOWN

To properly and safely shutdown the actuator, controller system and the pump system located in BEL 125 at the University of Idaho perform the following steps.

- 1) After the test has been stopped, click the “System Shutdown” button located in the “All in One” panel shown in Figure A-5. Push yes to all questions asking to turn high pressure and low pressure off. The pump should now be off and silent.
- 2) Exit the SW Application on the computer and push yes to the dialog box asking to shut down the controller engine.
- 3) Turn off power to both of the pumps by lowering the levers shown in Figure A-2.
- 4) Turn off the pump coolant water valve shown in Figure A-1 by turning it to the right.
- 5) The computer, pump, and water should not be making any noise and are now safely powered down.

APPENDIX-B: SUPPLEMENTARY DATA SHEETS FOR MATERIALS AND TESTING

FILE COPY



PRE-MIX, INC.
6901 SR 270 PULLMAN, WA 99163

CONCRETE
(509) 872-2200
SAND & GRAVEL

CAUTION: May cause eye or skin injury. Contains Portland cement. Freshly mixed cement, mortar, concrete, or grout may cause skin injury. Avoid contact with skin where possible, and wash exposed skin areas promptly with water. If any cement or cement mixtures get into the eye, rinse immediately and repeatedly with water and get prompt medical attention.

LIMITED WARRANTY
• The only liability of Pre-Mix Inc. for product defect is the return of the purchase price.
• In no event shall Pre-Mix, Inc. be liable for any direct, indirect, incidental or consequential damages resulting from the use of the products or arising out of breach of any warranty.
• All claims for damages or shortages must be made within 24 hours of delivery.

UNLOADING
Free unloading time 7 1/2 minutes per cubic yard of concrete. Charge thereafter at posted truck time rates. This concrete designed in accordance with specifications indicated below

We make deliveries inside the curb line at customer's risk only and accept no responsibility whatsoever for damages resulting from such deliveries.

REASON FOR DELAY

ARRIVED EARLY WHEEL BARROW
 ADDED WATER WAITING FOR TRUCK TO UNLOAD
 JOB NOT READY LACK OF HELP
 OTHER

		START REV	FINISH REV				
LEAVE PLANT	ARRIVE JOB SITE	START DISCHARGE	FINISH DISCHARGE	ARRIVE PLANT	YES <input type="checkbox"/>		
8:15	8:30	:	:	:	NO <input type="checkbox"/>		
<p>A LATE CHARGE EQUAL TO THE MAXIMUM ALLOWED BY LAW BUT NOT LESS THAN 18% ANNUAL PERCENTAGE RATE WILL BE CHARGED ON ALL PAST DUE ACCOUNTS.</p>			REC'D BY X	TEST CYLINDERS TAKEN			
			ADDITIONAL WATER ADDED TO THIS CONCRETE WILL REDUCE ITS STRENGTH				
			ARRIVED AT JOB WITH _____ INCH SLUMP ADDED _____ GAL WATER AT CUSTOMER REQUEST.				
ORDER NO.	CUST. NO.	PMI PRJ. NO.	CUSTOMER P.O./JOB NO.	TICKET NO.	DRIVER		
12708	MOT_NO			54242			
CUSTOMER			DELIVERY ADDRESS		DATE		
MOTLEY-MOTLEY, INC.			ENGINEERING BUILDING		09/21/2017		
DELIVERY INSTRUCTIONS							
LOAD QTY	DLVD QTY	ORDER QTY	PRODUCT CODE	PRODUCT DESCRIPTION	UNIT PRICE	AMOUNT	
1.75	1.75	1.75	1184+1	9 SK 3/4 AGG W/WRA			
LOAD SIZE	MIX NO.	MIX DESCRIPTION	SLUMP	USE	TRUCK	SALES TAX	TOTAL DUE
1.75	1184+1	9 SK 3/4 AGG W	4.00	BEAM	122		
Material	Design Qty	Required	Batched	% Var	% Moisture	Actual Wat	
3/4" CUBED	1725 lb	3025 lb	3060 lb	1.16%	0.20% M	1 gl	
BLEND SAND	1450 lb	2735 lb	2880 lb	+ 5.28%	7.80% A	25 gl	
TYPE I-II	846.0 lb	1480.5 lb	1490.0 lb	0.64%			
DARAVAIR	3.00 oz	5.25 oz	5.00 oz	-4.76%			
DARACEM	50.00 oz	87.50 oz	87.00 oz	-0.57%			
WATER	33.0 gl	35.1 gl	33.0 gl	-5.86%		33.0 gl	

Figure B-14 Pre-Mix Concrete Plant HSC Mix Material Quantities

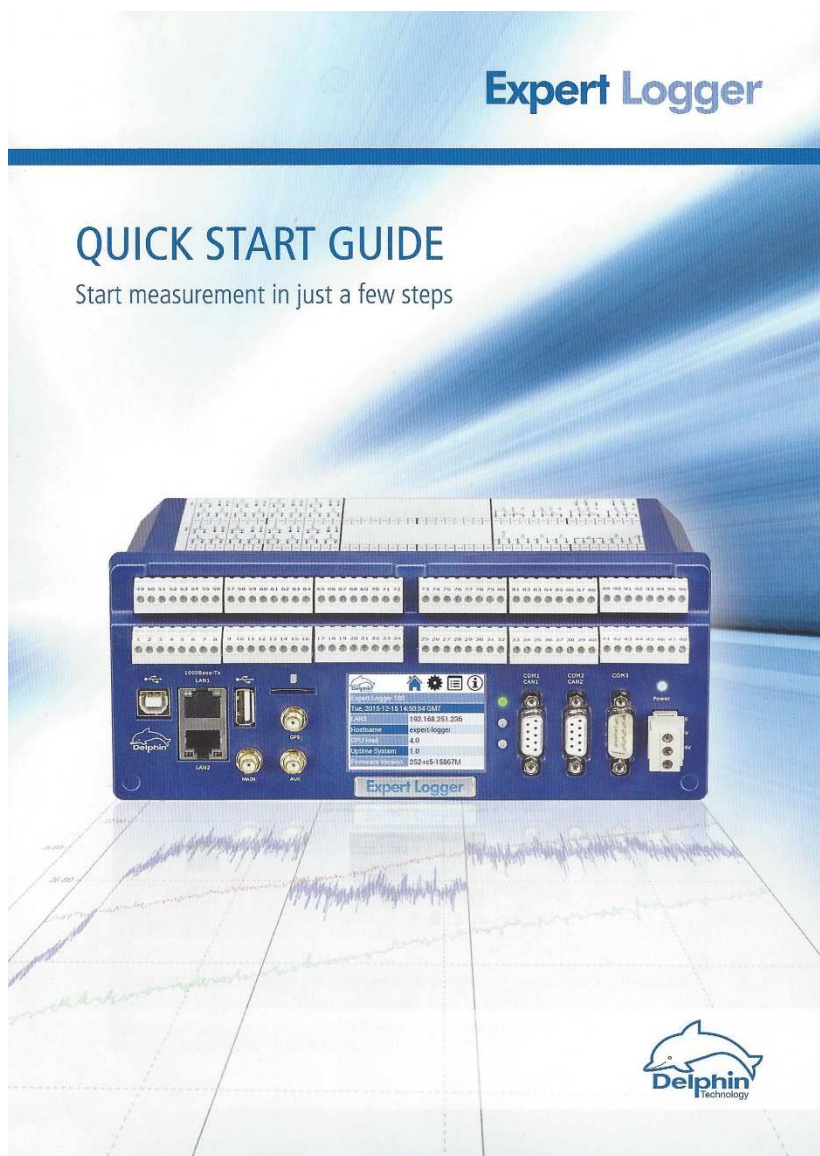


Figure B-15: Delphin Expert Data Logger Information Manual Display

VPG MICRO - MEASUREMENTS **MICRO MEASUREMENTS**
PERFORMANCE THROUGH PRECISION
micro-measurements@vishaypg.com
http://www.micro-measurements.com
A VPG Brand

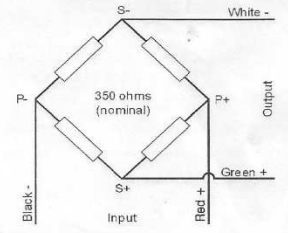
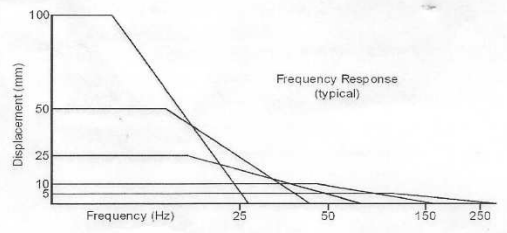
Calibration Report for Linear Displacement Sensor

Model	HS50	Serial Number	MG50892354
Test Date	11.12.2016		

Calibration Data	
Rated (Full Scale) Displacement	50.000mm
Rated (Full Scale) Output	3.033mV/V
Linearity Error	0.34%

Tested at 20°C nominal.
Displacement standards traceable to NIST

Additional Information



Excitation Volts: 2 to 10VDC

Figure B-16: Micro Measurements LVDT Data Sheet

MEME® MICRO-MEASUREMENTS
FOR COMPLETE TECHNICAL DATA, VISIT WWW.VISHAYPG.COM

GRID RESISTANCE IN OHMS		TC OF GAGE FACTOR, %/100°C
350.0±0.6%		(+1.2±0.2)

GRID	GAGE FACTOR @ 24°C	TRANSVERSE SENSITIVITY
1	2.150±0.5%	(-0.6±0.2)%
2		
3		
NOM		


THERMAL OUTPUT COEFFICIENTS FOR 1018 STEEL @ G.F. OF 2.00		
ORDER	FAHRENHEIT	CELSIUS
0	-1.95E+2	-7.61E+1
1	+4.71E+0	+5.04E+0
2	-3.33E-2	-8.56E-2
3	+7.51E-5	+4.04E-4
4	-4.59E-8	-4.81E-7
5		

FOL LOT NUMBER
A86AD439

WORK ORDER NUMBER
08240269
32388050

ITEM CODE	QTY 1 PK	CODE	RoHS COMPLIANT
MMF321934	(1 pcs)	201640US	

COUNTRY OF ORIGIN USA



C2A-06-20CLW-350

Figure B-17: Micro Measurements Strain Gauge Data Sheet